

**STUDY OF OSTWALD RIPENING OF SUPPORTED METAL
NANOPARTICLES IN VARIOUS ORGANIC MEDIUM**

TAN QIU LING

**A project report submitted in partial fulfilment of the
requirements for the award of Bachelor of Engineering
(Hons.) Chemical Engineering**

**Lee Kong Chian Faculty of Engineering and Science
Universiti Tunku Abdul Rahman**

September 2018

DECLARATION

I hereby declare that this project report is based on my original work except for citations and quotations which have been duly acknowledged. I also declare that it has not been previously and concurrently submitted for any other degree or award at UTAR or other institutions.

Signature : _____

Name : Tan Qiu Ling

ID No. : 1500603

Date : _____

APPROVAL FOR SUBMISSION

I certify that this project report entitled “**STUDY OF OSTWALD RIPENING OF SUPPORTED METAL NANOPARTICLES IN VARIOUS ORGANIC MEDIUM**” was prepared by **TAN QIU LING** has met the required standard for submission in partial fulfilment of the requirements for the award of Bachelor of Engineering (Hons.) Chemical Engineering at Universiti Tunku Abdul Rahman.

Approved by,

Signature : _____

Supervisor : _____

Date : _____

Signature : _____

Co-Supervisor : _____

Date : _____

The copyright of this report belongs to the author under the terms of the copyright Act 1987 as qualified by Intellectual Property Policy of Universiti Tunku Abdul Rahman. Due acknowledgement shall always be made of the use of any material contained in, or derived from, this report.

© 2018, Tan Qiu Ling. All right reserved.

ACKNOWLEDGEMENTS

I would like to express my special thanks and gratitude to my supervisor, Dr Yap Yeow Hong for his benevolent patience, encouragements and guidance that is invaluable to me for completing this project. Without his guidance and generous advice, this report would not have been possible.

I would like to thank everyone who had contributed to the successful completion of this project. I would like to express my gratitude to my senior, Wong Farng Hui for her invaluable advice, guidance and enormous patience while I am facing various sort of problems.

In addition, I would also like to express my gratitude to my loving parents and friends who had helped and given me encouragement.

Lastly, I would like to express my thanks and appreciations to everyone who helped me out in direct or indirect way to complete this report.

ABSTRACT

Ostwald ripening is one of the major deactivation problems that cause the loss of catalytic activity over time resulting in shortened catalysts lifetime owing to the loss of active sites on catalysts surface. In the case of Ostwald ripening, the metal nanoparticles dissolve into the solution and then redeposit onto the surface to form larger particles. This project aims to investigate the effect of different organic medium used for hydrogenation reaction on the deactivation of the catalyst. Four types of organic medium which are CPO, lauric acid, SPSFA and citral were used for hydrogenation reaction. Extensive comparisons between fresh and spent catalyst in terms of characteristics and catalytic activity were conducted. The results shown that catalyst used for hydrogenation of CPO suffered the most severe deactivation which is mainly due to the presence of calcium poisons in CPO. EDX analysis and ICP-OES analysis have shown that catalyst for hydrogenation of SPSFA lost the most significant amount of nickel which can be attributed to Ostwald ripening while the loss of nickel is less significant for hydrogenation of other organic mediums. The significant loss of nickel in SPSFA might be due to its higher acidity as compared to other organic medium which tends to leach the nickel. The compositions of each organic sample were quantified using GC-FID. The unsaturated fatty acids in CPO, lauric acid and SPSFA were successfully converted into the corresponding saturated fatty acids while for citral, the composition changes from neral to citronellol after hydrogenation. The steep IV drop and very low IV have shown that the catalysts gave better performance in the hydrogenation of SPSFA and lauric acid with less deactivation. On the other hand, the smooth and steady IV drop for hydrogenation of CPO has indicated poor catalytic activity as a result of rapid deactivation which is in agreement with the characterization results.

TABLE OF CONTENTS

DECLARATION	II
APPROVAL FOR SUBMISSION	III
ACKNOWLEDGEMENTS	V
ABSTRACT	VI
TABLE OF CONTENTS	VII
LIST OF TABLES	IX
LIST OF FIGURES	X
LIST OF SYMBOLS/ ABBREVIATION	XIII
LIST OF APPENDICES	XIV

CHAPTER

1	INTRODUCTION	1
	1.1 General Introduction	1
	1.2 Problem Statement	3
	1.3 Aims and Objectives	5
	1.4 Scope of Study	5
2	LITERATURE REVIEW	6
	2.1 Catalyst Deactivation	6
	2.1.1 Poisoning	6
	2.1.2 Coking, Carbon Deposition and Fouling	11
	2.1.3 Thermal Degradation and Sintering	15
	2.1.4 Other Mechanisms of Deactivation	18
	2.2 Ostwald Ripening	20
	2.2.1 Thermodynamic Driving Force for Ostwald ripening	20
	2.2.2 Theory of Ostwald Ripening	23
	2.2.3 Factors Affecting Ostwald Ripening	26
	2.2.4 Examples of Catalytic Reactions with Ostwald Ripening	30
	2.3 Hydrogenation Reaction	34

	2.3.1	Fats and Fatty Acids	34
	2.3.2	Citral	40
3		METHODOLOGY	43
	3.1	Materials	43
	3.2	Partial Hydrogenation Process	43
	3.3	Spent Catalyst Collection	46
	3.4	Catalyst Performance Evaluation	47
	3.4.1	Iodine Value (IV) Test	47
	3.4.2	Gas Chromatography (GC) Analysis	48
	3.5	Characterization of Catalyst	52
	3.5.1	Scanning Electron Microscopy with Energy Dispersive X-ray Spectroscopy (SEM-EDX)	53
	3.5.2	Inductively Coupled Plasma Optical Emission Spectroscopy (ICP-OES)	54
4		RESULTS AND DISCUSSION	56
	4.1	Weight Loss of Spent Catalysts Before and Roasting	56
	4.2	Characterization of Catalyst	57
	4.2.1	Scanning Electron Microscopy with Energy Dispersive X-ray Spectroscopy (SEM-EDX)	57
	4.2.2	Inductively Coupled Plasma Optical Emission Spectroscopy (ICP-OES)	62
	4.3	Catalyst Performance Evaluation	63
	4.3.1	Iodine Value (IV)	65
	4.3.2	Gas Chromatography (GC) Analysis	68
5		CONCLUSION	71
	5.1	Conclusions	71
	5.2	Recommendations for Future Work	72
		REFERENCES	73
		APPENDICES	77

LIST OF TABLES

Table 2.1:	Catalyst Poisons (Figueiredo, Pereira and Faria, 2008)	8
Table 2.2:	Common poisons for catalysts used in different types of processes.(Bartholomew, 2001)	9
Table 2.3:	Possible volatile metal compounds generated in catalytic processes. (Bartholomew and Farrauto, 2006)	18
Table 2.4:	Major Saturated Fatty Acids (Nikita, n.d.)	35
Table 2.5:	Major Unsaturated Fatty Acids (Nikita, n.d.)	36
Table 2.6:	Refining process for crude palm oil (CPO) (Shahidi, 2005)	38
Table 3.1:	Operating conditions for hydrogenation process	44
Table 4.1:	Weight of spent catalyst before and after	56
Table 4.2:	EDX elemental composition of fresh and spent Ni/SiO ₂ catalyst collected after the hydrogenation of different organic medium	61
Table 4.3:	ICP-OES elemental analysis of spent catalyst sample	63
Table 4.4:	IV test result for CPO, lauric acid, SPSFA hydrogenated in the presence of Ni/SiO ₂ catalysts	66
Table 4.5:	Percentage composition of fatty acids present in CPO, lauric acid, SPSFA before and after hydrogenation	69
Table 4.6:	Percentage composition of citral during hydrogenation at different time interval	70

LIST OF FIGURES

Figure 1.1:	Energy Profile Diagram (Khan Academy, n.d.)	1
Figure 1.2:	Supported Metal Nanoparticles	2
Figure 1.3:	Illustration of Ostwald ripening (a) and Particle Migration (b)	4
Figure 2.1:	Conceptual two-dimensional model of metal catalyst poisoned by sulphur atoms in ethylene hydrogenation process (Bartholomew, 2001)	11
Figure 2.2:	Schematic of decay by coking (Fogler, 2011)	12
Figure 2.3:	Possible effects of fouling and coking on supported metal catalysts. (Bartholomew, 2001)	12
Figure 2.4:	Different mode of coking deactivation on zeolites: (a) and (b) shows pore blocking in mordenite and three-dimensional erionite, respectively; (c) site coverage; (d) site accessibility hindered by channel blocking; (e) pore blocking by exterior deposits. (Boskovic and Baerns, 2004)	13
Figure 2.5:	Formation, transformation and gasification of carbon on nickel catalyst (a, g, s refer to adsorbed, gaseous and solid states, respectively). (Elsevier, 1983)	14
Figure 2.6:	Illustration of sintering via particle migration: (1) particle diffusion; (2) particle coalescence. (Berg, 2016)	16
Figure 2.7:	The decay rate and the mechanisms involved in three stages of catalyst sintering. (Hansen <i>et al</i> , 2013)	17
Figure 2.8:	Schematic illustration of a particle on flat surface (Berg, 2016)	21
Figure 2.9:	Illustration of particle growth via Ostwald ripening. Metal particle is represented by blue color while the support is shown in grey. Metal atoms diffusing through reaction medium and support surface are in green and red respectively. (Berg, 2016)	23

Figure 2.10:	Typical line shape of particle size distribution based on LSW Theory. (Rao, Muller and Cheetham, 2006)	25
Figure 2.11:	TEM images of the same area on the model catalyst Co/SiO ₂ before (a) and after (b) the exposure to FTS condition. Blue circles indicate the particles which have shown significant decrease in size during FTS while red circles indicate the particles which have disappeared during FTS.(Kistamurthy <i>et al.</i> , 2015)	33
Figure 2.12:	Structure of Fats	34
Figure 2.13:	Hydrogenation of Oleic Acid (Ophardt, 2003)	36
Figure 2.14:	General Hydrogenation Scheme of Linolenic Acid	37
Figure 2.15:	Refining process for crude palm oil (CPO)	38
Figure 2.16:	Reaction schematic of fat splitting process	40
Figure 2.17:	Structure of Geranial and Neral	41
Figure 2.18:	Reaction Scheme for Hydrogenation of Citral (Maki-Arvela <i>et al.</i> 2003)	42
Figure 3.1:	Reactor for Hydrogenation Process	45
Figure 3.2:	Dried acetone-washed spent catalysts collected from hydrogenated citral, CPO, lauric acid and SPSFA (from left to right).	46
Figure 3.3:	Roasted acetone-washed spent catalysts collected from hydrogenated citral, CPO, lauric acid and SPSFA (from left to right).	46
Figure 3.4:	Esterification of fats under reflux	50
Figure 3.5:	Crude palm oil (CPO) from partial hydrogenation after esterification and dissolved in dichloromethane.	50
Figure 3.6:	Lauric acid from partial hydrogenation after esterification and dissolved in dichloromethane.	51
Figure 3.7:	Splitted palm stearin fatty acid (SPSFA) from partial hydrogenation after esterification and dissolved in dichloromethane.	51

Figure 3.8:	PerkinElmer Clarus 500 Gas Chromatography	51
Figure 3.9:	Agilent Technologies 7890B Gas Chromatography	52
Figure 3.10:	Hitachi S-3400N scanning electron microscope	53
Figure 3.11:	PerkinElmer optical emission spectrometer Optima 7000 DV	55
Figure 4.1:	SEM image of fresh Ni/SiO ₂ catalyst (magnification x5500)	58
Figure 4.2:	SEM image of roasted acetone-washed spent Ni/SiO ₂ catalyst collected from CPO (magnification x3500)	58
Figure 4.3:	SEM image of roasted acetone-washed spent Ni/SiO ₂ catalyst collected from lauric acid (magnification x5000)	59
Figure 4.4:	SEM image of roasted acetone-washed spent Ni/SiO ₂ catalyst collected from SPSFA (magnification x3200)	59
Figure 4.5:	SEM image of roasted acetone-washed spent Ni/SiO ₂ catalyst collected from citral (magnification x3200)	60
Figure 4.6:	Dissolution of Nickel in Fatty Acids (Hawkins, 2013)	62
Figure 4.7:	Crude Palm Oil (CPO) before (a) and after 30 minutes, 60 minutes, 120 minutes and 180 minutes (b, c, d, e) hydrogenation reaction, respectively.	64
Figure 4.8:	Lauric acid before (a) and after 30 minutes, 60 minutes, 120 minutes and 180 minutes (b, c, d, e) hydrogenation reaction, respectively.	64
Figure 4.9:	Splited palm stearin fatty acid (SPSFA) before (a) and after 30 minutes, 60 minutes, 120 minutes and 180 minutes (b, c, d, e) hydrogenation reaction, respectively.	65
Figure 4.10:	Citral before (a) and after 30 minutes, 60 minutes, 120 minutes and 180 minutes (b, c, d, e) hydrogenation reaction, respectively.	65
Figure 4.11:	IV test result for CPO, lauric acid, SPSFA hydrogenated in the presence of Ni/SiO ₂ catalysts	66

LIST OF SYMBOLS/ ABBREVIATION

D	metal dispersion (%)
n	stoichiometry factor
M	metal loading (wt%)
$V_{adsorbed}$	volume of gas adsorbed ($\mu\text{mol/g}$)
$V_{gas,s.t.p}$	volume of gas at standard temperature and pressure (dm^3/g)
A_m	metal surface area (m^2)
N_A	Avogadro's number (atoms/mol)
a	cross sectional area of metal atom (m^2)
a_m	area of a metal atom on sample surface (m^2)
V_m	volume occupied by an atom (m^3)
ρ	atomic mass density (g/m^3)
IV	iodine value
GC	gas chromatography
SEM	scanning electron microscopy
EDX	energy dispersive X-ray spectroscopy
ICP-OES	Inductively coupled plasma optical emission spectroscopy

LIST OF APPENDICES

APPENDIX A:	Preparation of Solutions Used in ICP-OES	77
APPENDIX B:	Raw Data of EDX	80
APPENDIX C:	Calculation for Amount of Fatty acids Required and IV Test	96

CHAPTER 1

INTRODUCTION

1.1 General Introduction

Catalysts are substances that have been used in a large portion of chemical industry since 18th century. There are two types of catalysts: homogenous and heterogeneous. Homogeneous catalyst exists in the same phase as reactants. Heterogeneous catalyst involves the reaction of species in different phases. The demand of catalysts has increased significantly due to the rapid development of the chemical manufacturing. Undoubtedly, catalysts are indispensable part in most of the industrial processes because of the benefits they give. Catalysts provide larger surface for reactant molecules to attach to, resulting in the increase of probability of reaction. They are able to increase the rate of chemical reaction without being consumed by the reaction itself. That is, the catalysts will remain unchanged at the end of the catalyzed reaction. In general, catalysts help to save time and energy by lowering the activation energy required for the reaction to occur. They allow the reaction to take place at a much lower temperature.

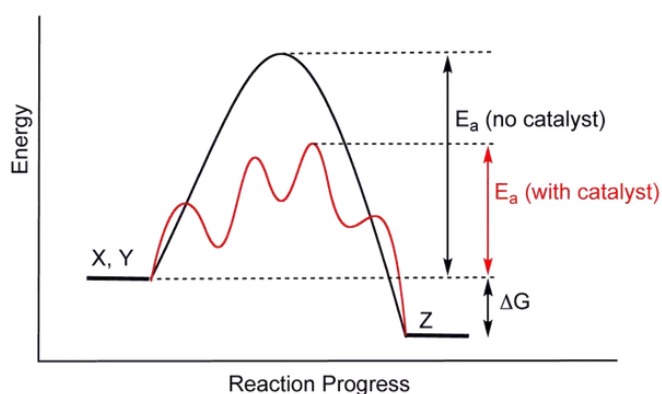


Figure 1.1: Energy Profile Diagram (Khan Academy, n.d.)

Figure 1.1 above shows the energy profile diagram of a reaction with and without using of catalysts. The presence of catalysts provides an alternative reaction pathway which requires lower activation energy as compared to the reaction pathway without using catalyst. In the meantime, the final outcome and the overall thermodynamics from reactants to products are the same for both pathways.

Although catalysts in theory are said to remain unchanged throughout the reaction, in reality catalysts can be inhibited, deactivated or destroyed. This undesirable phenomenon is known as deactivation. Catalyst deactivation is one of the major problems that occur simultaneously with the main reaction in most of the industrial catalytic processes. It results in the deterioration in catalytic activity or probably selectivity over time. A variety of mechanisms in chemical, mechanical and thermal terms may give rise to catalyst deactivation. These mechanisms can be categorized into three main groups: (i) poisoning, (ii) coking or fouling, and (iii) sintering. They may take place separately or in combination, but their net effect is always the removal of active surface area on the catalyst. Other mechanisms of deactivation include loss of active catalytic component through volatilization and mechanical damage such as erosion and attrition can be important in some instances (Bartholomew, 2001).

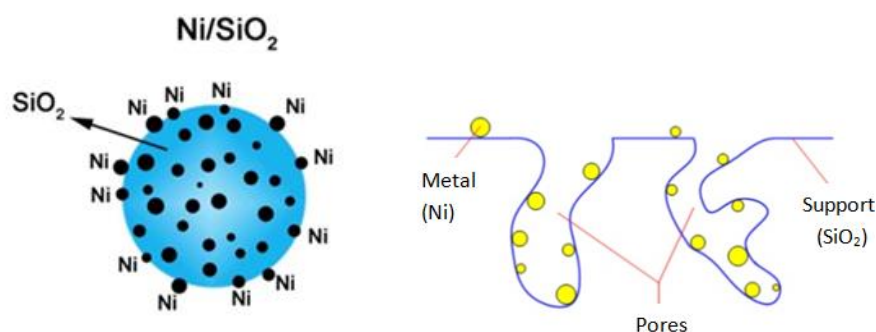


Figure 1.2: Supported Metal Nanoparticles

Recently, supported metal nanoparticles are widely used as catalyst in several industrial processes as compared to bulk metallic catalysts. Supported metal nanoparticles generally consist of metal nanoparticles from transition metal or noble metal that are dispersed and deposited on a porous support material (Hansen *et al*,

2013). The catalytic performance of supported metal nanoparticles can be affected by a variety of factors and particle size is an important consideration in determining catalytic reactivity. As particle size decreases, the surface area per unit mass increases, resulting in better catalytic activity since all chemical reactions take place on the catalyst surface. Additionally, other parameters including structure, morphology, chemical composition, oxidation state and chemical or physical environment are also considered to be pivotal role in the performance of catalysts (Argyle and Bartholomew, 2015).

Despite the advantage of large specific surface area, the supported metal nanoparticles are associated with large surface energy. This makes the nanoparticles tend to sinter and coalesce into larger particles in order to reach a more thermodynamically stable state (Hansen *et al*, 2013). Sintering, also known as thermal deactivation, is one of the ubiquitous problems that cause unwanted reduction in active surface area. It further results in the reduction of catalyst activity, especially catalytic processes operated at high temperature. In general, the growth of nanoparticles can occur through two mechanisms: (i) particle migration and (ii) atom migration. In the first case, the entire nanoparticles migrate along the surface of the support and then collide and coalesce with other nanoparticles. In the second case, the atoms escape from one nanoparticle, diffuse over the support surface until they collide with another nanoparticle (Bartholomew, 2001). This mechanism is often known as Ostwald ripening. In this work, while various deactivation mechanisms will be discussed, attention will be paid to Ostwald ripening of supported metal nanoparticles.

1.2 Problem Statement

Catalyst deactivation has great impact on the development, design and operation of industrial chemical reactors. As time scale for industrial catalytic deactivation can vary in the range of seconds (e.g. fluidized catalytic cracking) up to decade (e.g. ammonia synthesis), a catalyst developer may need to know the time scale of the catalyst deactivation in order to decide what reactor to use (Moulijn, Diepen and

Kapteijn, 2001). Deactivation results in the loss of active area on catalyst surface and thereby cause a decrease in catalyst lifetime and its performance in the reaction. This phenomenon may contribute to a strong negative impact on economy of the process as a result of the decrease in production rate. Due to this reason, extensive studies will need to be carried out to better understand catalyst deactivation in both chemical and physical aspects in order to design a more deactivation-resistant catalyst in the future.

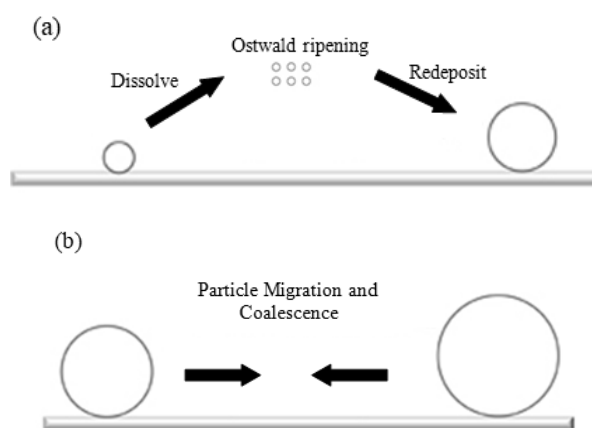


Figure 1.3: Illustration of Ostwald ripening (a) and Particle Migration (b)

In Ostwald ripening, the larger particles grow at the expenses of small particles until the small particles completely disappear. As a result of this phenomenon, the nanoparticles grow in size and the density of nanoparticles on the support surface is decreased. Numerous studies have shown that Ostwald ripening can be influenced by several parameters such as temperature, type of metal, support and promoter, and chemical environment (i.e. type of reactants). However, studies on the effect of the type of reactants on the extent of Ostwald ripening are still very limited. A more detailed understanding of this parameter on the catalyst deactivation will contribute to design of more robust catalysts with longer catalyst lifetime.

1.3 Aims and Objectives

The present study aims to address the problem of Ostwald ripening in the hydrogenation catalysts. This is done by studying the hydrogenation of different organic medium with the use of commercial nickel catalysts. In general, there are three objectives to be achieved in this study:

1. To compare the performance of catalyst in different organic mediums.
2. To investigate the extent of catalyst deactivation and in particular Ostwald ripening of catalysts through characterization of fresh and spent supported metal catalysts.

1.4 Scope of Study

The degree of Ostwald ripening can be quantified by several parameters including particle size of active phase, particle size distribution and dispersion. In this study, supported metal nanoparticles are characterized using techniques relevant to study the textural and structural properties, for instance, Scanning Electron Microscopy (SEM), Energy Dispersive X-ray Spectroscopy (EDX), and Inductively Coupled Plasma Optical Emission Spectroscopy (ICP-OES). Hydrogenation reactions were carried out to study the effect of different organic medium on the deactivation of the catalysts. While pulse chemisorption and Transmission Electron Microscopy (TEM) are highly relevant to the study of Ostwald ripening, the lack of access to these facilities limit the result and analyses that can be used to form a good conclusion on the extent of Ostwald ripening.

CHAPTER 2

LITERATURE REVIEW

2.1 Catalyst Deactivation

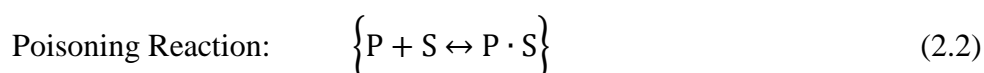
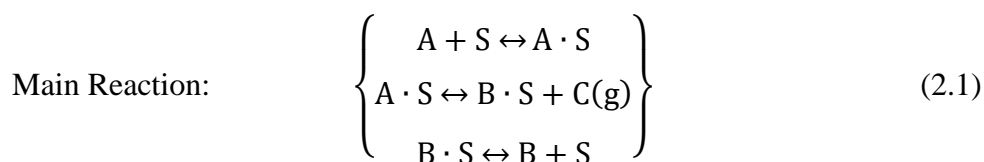
Deactivation is one of the major problems that cause the loss of catalytic activity over time resulting in shortened catalysts lifetime. It is a complex phenomenon which takes place concurrently with the main reactions. Basically, catalyst deactivation occurs owing to the loss of active sites on catalysts surface either resulted by chemical or physical reasons. Catalyst deactivation is said to be unavoidable in most processes. However, some of the negative impacts it caused may be prevented or postponed and sometimes even reversed. In the review by Bartholomew (2001), catalyst deactivation can be divided into four main groups, namely poisoning, coking or fouling and thermal degradation or sintering. These deactivation processes are individual effects whereas they may take place in combination or sometime one of the deactivation process initiate the dominating one. In the following sections, a brief description of the various mechanisms for catalyst deactivation will be given.

2.1.1 Poisoning

Poisoning is an important and difficult problem in a number of industrial catalytic processes. This process is attributed to the strong chemisorption of some substances on the surface of catalysts, resulting in a rapid reduction of the number of active sites (Fogler, 2011). The attached active sites become unavailable for the adsorption of reactants. A catalyst can be completely deactivated by just a small amount of poisons.

A poison may be a reactant, product of the reaction or impurity present in the feed stream. The adsorption strength of the substance compared to other competing substance decides if it acts as a poison in a reaction. Take oxygen, for example, in the process where ethylene is partially oxidized on silver catalysts, it can be a reactant whereas in hydrogenation of ethylene on nickel catalyst, it is a poison. Poison results in the reduction of number of active sites available for reaction. Apart from physically blocking the active surface area, adsorbed poison may act by altering in geometric or electronic properties (Bartholomew, 2001).

In a simple kinetic model, the poisoning process by an impurity, P, presents in the feed stream can be shown by the following equations:



Where A, B and S are reactants, products, and active sites, respectively. P · S represents strongly adsorbed poison (Fogler, 2011).

Figueiredo, Pereira and Faria (2008) found that poisoning involves the reaction of poisons with surface active sites thereby the type of poison largely relies on the nature of the active sites. For group VIII metal catalysts, the chemicals in groups VA and VIA are typical poisons. The free radical exists on the surface metal atoms make them involve in the adsorption of reactants as well as poisons. Chemicals containing unoccupied orbitals, unshared electron pairs or more metal ions with than four d- electrons may act as poisons for metals. Moreover, substances having multiple bonds, for example, carbon monoxide, dienes and acetylene, are one of the potential poisons. In general, metal oxide-based catalysts have higher resistance to poisoning as compared to metal catalysts. According to Table 2.1, acid catalysts can be poisoned by bases. Compounds like As, Pb and Cd may act as poisons for oxide catalysts. They adsorb on the active sites and cause the active sites becomes permanently inactive. Due to the capability of active sites of non-stoichiometric oxides to accept or donate electrons, molecules which have the ability

to alter the most favourable oxidation state of the ions on surface may be considered as poison (Figueiredo, Pereira and Faria, 2008).

Table 2.1: Catalyst Poisons (Figueiredo, Pereira and Faria, 2008)

Catalyst	Active Sites	Poisons
Metals	Exposed metal atoms	Molecules containing elements of groups 15 or 16 with unshared electrons pairs; Molecules with multiple bonds
Acids	Lewis or Bronsted acid centers	Basic molecules in the feed; basic impurities in the solid
Non-stoichiometric oxides	Coordinatively unsaturated surface ions	Any substance capable of changing the most favourable oxidation state of surface ions

Table 2.2 shows the common poisons for some industrial catalytic processes. Based on Table 2.2, the compounds containing sulphur or arsenic are common poisons for several reactions including hydrogenation, dehydrogenation and steam reforming. Meanwhile, the acidic solids like silica-alumina and zeolites are normally poisoned by organic compounds and ammonia. Similarly, a variety of reactions including catalytic cracking and hydrotreating can be poisoned by metal compounds such as Ni, Pb, Pt and V (Bartholomew, 2001).

Table 2.2: Common poisons for catalysts used in different types of processes.(Bartholomew, 2001)

Reaction	Catalyst	Poisons
Catalytic Cracking	Silica-alumina, Zeolites	Organic bases, hydrocarbons heavy metals
Hydrogenation, dehydrogenation	Ni, Pt, Pd	Compounds of S, P, As, Zn, Hg, halides, Pb, NH ₃ , C ₂ H ₂
Steam reforming of methane	Ni	H ₂ S, As
Ammonia synthesis	Fe or Ru	O ₂ , H ₂ O, CO, S, C ₂ H ₂
Fischer-Tropsch synthesis	Co or Fe	H ₂ S, COS, As, NH ₃ , metal carbonyls
Hydrocracking	Noble metals on zeolites	NH ₃ , S, Se, Te, P
Ethylene oxidation to ethylene oxide	Ag	C ₂ H ₂
Oxidation selective catalytic reduction	V ₂ O ₅	As, Fe, K, Na from fly ash
Oxidation of CO and hydrocarbons	Pt, Pd	Pb, P, Zn, SO ₂ , Fe
Hydrotreating of residue	Co and MoO ₃	Asphaltenes, N compounds, Ni, V

Poisoning can be classified as reversible or irreversible. The former case takes place when the adsorption strength of the poison on the catalyst active sites is not too great. The poisoned catalyst can be regenerated through the removal of the poison source from the feed stream. For example, the feed stream containing nitrogen compounds may lead to deactivation on catalyst acidic sites. The effects are undesirable yet they are temporary and can be eliminated with removal of nitrogen from the feed. On the other hand, when the poison attaches on the catalyst with great

adsorption strength, the effects are unable to be reversed. It is so called irreversible poisoning. The deactivation effects caused by poisons adsorbed on active sites are the same no matter the poisoning is either reversible or irreversible (Argyle and Bartholomew, 2015).

Another way to classify poisoning is based on their selectivity (Forzatti and Lietti, 1999). As in selective poisoning, the characteristics of adsorption sites may be distributed differently over the catalyst surface thereby leading to a complex interaction. The poison tends to adsorb on the most active sites at first so that there will be a variety of relationships between the amount of poisons adsorbed with the catalytic activity. For non-selective poisoning, the poison is uniformly adsorbed by the active sites. As a result, a linear function can be obtained for the correlation between amount of poison adsorbed and catalytic activity (Bartholomew, 2001).

Figure 2.1 shows a conceptual two-dimensional model of metal catalyst poisoned by sulphur in ethylene hydrogenation process (Argyle and Bartholomew, 2015). According to Figure 2.1, poison may lead to deactivation effects in several mechanisms. The first effect is often called geometric effect. A sulphur atom is strongly adsorbed on the metal surface and blocks the adsorption site. Second, due to electronic interaction, the electronic properties of catalyst are changed by poison. The sulphur atom electronically decreases the abilities of near-by neighbour active sites to chemisorb reactant molecules which are hydrogen and ethylene in this case (Baerns, 2004). Third, the catalytic properties may be changed dramatically through the restructuring of the surface. The restructuring process is carried out by the poison strongly adsorbed on catalyst surface and it is severe when the reaction is sensitive towards surface structure (Forzatti and Lietti, 1999). Moreover, the poison hinders the reactants adsorbed on active sites from accessing to one another and eventually postpones and inhibits the adsorbed reactants to diffuse on surface (Argyle and Bartholomew, 2015).

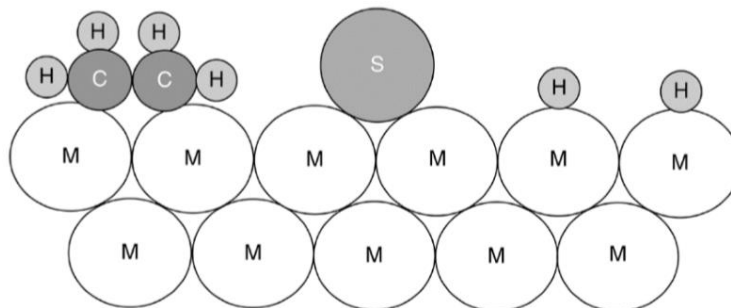


Figure 2.1: Conceptual two-dimensional model of metal catalyst poisoned by sulphur atoms in ethylene hydrogenation process (Bartholomew, 2001)

It is difficult to regenerate poisoned catalyst. Instead of regeneration, reduction of poisons present in feed stream may be the best approach to decrease the poisoning effects. This can be achieved by letting the feed to go through appropriate treatments. Additionally, by choosing catalyst with proper formulations and design, the poisoning deactivation can be inhibited. The catalyst design including surface area, pore size and shape can greatly affect the resistance of catalyst to poison. The operating conditions also are one the factors affecting the sensitivity of catalysts towards poisons (Forzatti and Lietti, 1999).

2.1.2 Coking, Carbon Deposition and Fouling

Fouling is a phenomenon where the catalyst surface is deposited and covered by undesired material. In catalytic reactions involving hydrocarbons or sometimes carbon oxides, undesired reactions may take place on the catalyst surface and form carbonaceous material. The pores as well as the active sites of the catalyst are physically blocked or plugged by the carbonaceous substances so that the opportunity of reactants to approach the active sites is impeded. With the decline in the amount of active sites exposed to surroundings, the catalyst is less active.

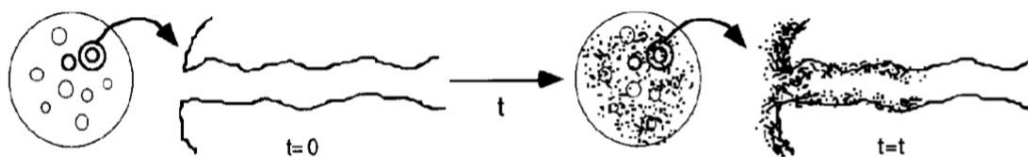


Figure 2.2: Schematic of decay by coking (Fogler, 2011)

The carbonaceous materials are commonly referred to carbon and coke. There are differences between coke and carbon while the definitions for both are somewhat arbitrary. In general, carbon is formed by disproportionation of carbon monoxide whereas coke is considered as the product of decomposition or condensation of hydrocarbons. These reactions will produce various carbon and coke in different morphology and reactivity. It is not easy to define the chemical nature of coke. Coke is a complex mixtures formed by different kinds of substances with different structures and origins. Any hydrocarbon molecules containing highly deficient hydrogen can act as a coke precursor. The coke may present in terms of large molecular weight hydrocarbons as well as primarily carbons based on the conditions where the coke is produced (Argyle and Bartholomew, 2001).

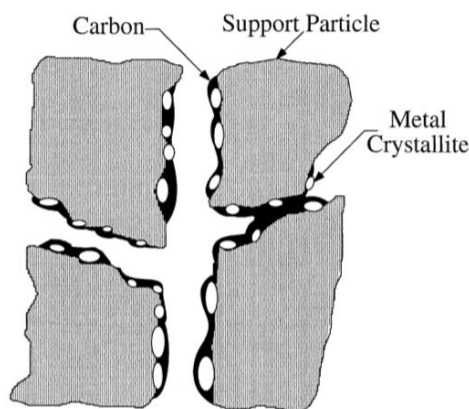


Figure 2.3: Possible effects of fouling and coking on supported metal catalysts. (Bartholomew, 2001)

Possible effects of fouling and coking on supported metal catalysts can be seen in Figure 2.3. Carbon may strongly adsorb as monolayer or multilayer resulting in the blockage of active surface area. The reactants are then hindered from accessing to active sites. Another effect is that the metal particle is completely encapsulated, leading to deactivation of that particle. Many crystallites plug the pores such that reactants are not able to access to these pores. Finally, either disintegration of supported metal catalyst or plugging of reactor voids may occur when strong carbon species build up in pores in so far as they stress and cause the support material to break (Argyle and Bartholomew, 2001).

Reaction conditions including temperature and reactant composition greatly influence the deactivation rate of a catalyst in reaction. Boskovic and Baerns (2004) has shown that the rate of carbon or coke to build up depends greatly on the catalyst structure such as metal species, metal size, support material, pore size and pore structure in certain conditions. Different modes of coking deactivation on zeolites are illustrated in Figure 2.4. Figure 2.4 (a) and (b) show the pore blocking in the case of mordenite and three-dimensional erionite, respectively. In contrast, in Figure 2.4 (c, d and e), deactivation initiate as acid sites coverage in three-dimensional channels without hole. As increase in the amount of coke, the deactivation takes place as blockage of sites in the intersections of the channel and then followed by blockage of pores by exterior deposits (Boskovic and Baerns, 2004).

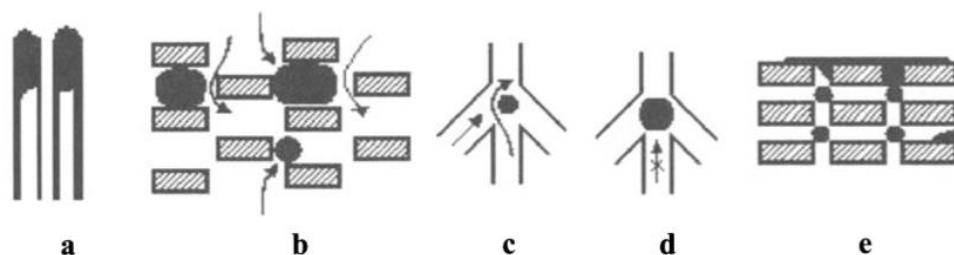


Figure 2.4: Different mode of coking deactivation on zeolites: (a) and (b) shows pore blocking in mordenite and three-dimensional erionite, respectively; (c) site coverage; (d) site accessibility hindered by channel blocking; (e) pore blocking by exterior deposits. (Boskovic and Baerns, 2004)

In a study by Bartholomew (2001), the mechanisms of carbon formation from CO dissociation on Ni catalyst have been reviewed. As shown in Figure 2.5, there are several kinds of carbon can be formed from the dissociation of CO, including adsorbed atomic carbon (C_{α}), polymeric or amorphous carbon (C_{β}), vermicular carbon (C_{ν}), bulk Ni carbide (C_{γ}), and crystalline, graphitic carbon (C_c) (Forzatti and Lietti, 1999). In the mean time, Forzatti and Lietti (1999) reported that three different types of carbon or coke species may be formed during the steam reforming of hydrocarbons over metal catalyst, namely encapsulating film, whisker-like and pyrolytic carbon. Encapsulated-like hydrocarbon is a product of slow polymerization of C_nH_m on metal catalyst at temperature below 500 °C. Whisker-like carbon is obtained from diffusion of carbon atoms through metal crystal followed by nucleation and growth of filaments with metal particles on top. Pyrolytic carbon is formed by cracking of hydrocarbons and deposition of carbon precursors (Forzatti and Lietti, 1999).

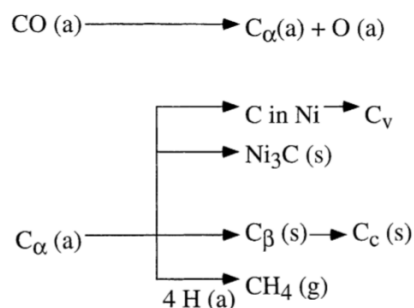


Figure 2.5: Formation, transformation and gasification of carbon on nickel catalyst (a, g, s refer to adsorbed, gaseous and solid states, respectively).(Elsevier, 1983)

By using catalyst with optimal composition under appropriate conditions, the fouling or coking deactivation may be controlled. Gasification process is one of the methods to remove coke decomposition. Gasifying agents such as hydrogen, steam and oxygen can convert materials containing carbon into methane, CO and CO_x compounds respectively. If the rate of coke removal by gasification is lower than the rate of coke formation, an appropriate regeneration approach such as combustion of deposited carbon or coke should be applied (Trimm, 1977).

2.1.3 Thermal Degradation and Sintering

When a catalyst containing metal nanoparticles is used in reaction, the nanoparticles may grow into larger size and this process is so called sintering. Sintering is commonly known as thermal deactivation or catalyst ageing. It generally takes place at elevated temperature, for example steam reforming. Supported metal nanoparticles have great ratio of surface area to volume. As a result, they are associated with large surface energy and thus in meta-stable state. As a means to lower the surface free energy, the metal crystallites grow and agglomerate into larger ones, leading to the loss in the surface area on the catalyst. Regarding supported metal catalyst, sintering not only may be indicated as the reduction in the number of active surface area due to agglomeration of the crystallites, but also refer to the loss of support or catalyst surface area caused by collapse of support or pore (Adibi, 2014.)

At microscopic level, this phenomenon is attributed to the migration of the metal atoms over the surface of the support material and their movements reflect to two different sintering mechanisms. The first mechanism is known as particle or crystallite migration where entire particle migrates across the support surface and collides or coalesces with other particles. Another mechanism is atomic migration or Ostwald Ripening. The difference between atomic and particle migration is that atomic migration initiated by the escape of metal atoms from the metal particles. The metal atoms first detach from particles and then migrate over the support surface. Lastly, the metal atoms are captured by other larger particles (Simonsen *et al.*, 2011). Figure 2.6 and Figure 2.9 show the simple illustration of these mechanisms.

In the case of sintering via particle migration, it is an irreversible process as the metal surface area decreases, leading to the increase in free energy. Berg (2016) reported that small particles with size of less than 25 nm coalesce more rapidly as the thermal stability increases with the use of supports as compared to diffusion. In most industrial catalytic processes, the rate limiting step for supported metal catalysts in this mechanism is diffusion of particle. For particles to come across and join together on a surface, the diffusion coefficient and the inter-particle distances are important. Meanwhile, the diffusion of particle may be influenced by particle size, metal-support interaction and also metal-reaction medium interaction. Additionally,

the inter-particle spacing and the interaction between metal particle and support depend on the support structure. For example, the metal particle is more stable on a concave surface than on a convex surface. The diffusion coefficients of the metal particles vary on different surface (Berg, 2016).

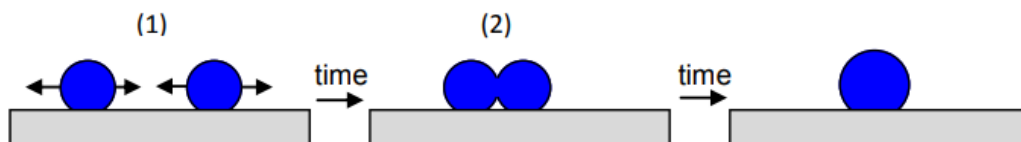


Figure 2.6: Illustration of sintering via particle migration: (1) particle diffusion; (2) particle coalescence. (Berg, 2016)

The diffusion of metal particles on the catalyst surface will result in accumulation on one side of the catalyst due to random fluctuations. The particle moves in a Brownian type motion on the support and the displacement of the particle can be estimated by performing on the equation provided:

$$x = 2\sqrt{D_p t} \quad (2.3)$$

where D_p represents the diffusion coefficient of the particle and t refer to time (Contreras and Fuentes, 2012).

In a review by Hansen *et al.* (2013), catalyst sintering can be divided into three phases. These mechanisms generally occur in sequence. At initial phase, the metal particles are the smallest in size and also the most active and selective in many cases. This process takes place within the first few hours. The number of surface area decreases rapidly with the diminishing of smaller particles. That is, the catalyst lost activity rapidly and it appears to be dominated by atomic migration in the initial stage of sintering for metal catalysts. The growth of particles in size can be observed in the later phases when the particles are close to each other and normally at higher temperature. As shown in Figure 2.7, sintering process slows down as the particles size as well as the interparticle separation increases. It eventually reaches stable

performance in phase III where the particles have become larger in size (Hansen *et al.*, 2013).

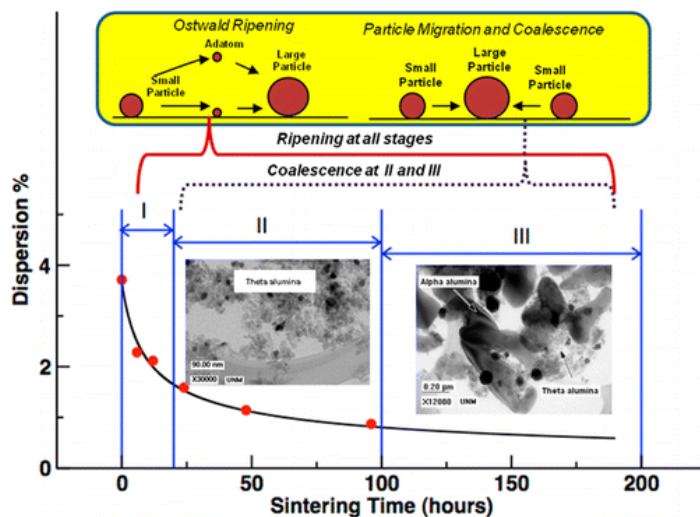


Figure 2.7: The decay rate and the mechanisms involved in three stages of catalyst sintering. (Hansen *et al.*, 2013)

It is found that the Brownian-like motion of particles is not dominant at moderate temperature. At lower temperature, atomic migration is favoured than particle migration. This is because the small cluster or atoms have higher diffusivities which make their migration easier than larger particles. The thermal energy required to initiate the movement of larger particles will only be obtained at higher temperature. Therefore, atomic migration starts in lower temperature and particle migration occurs once the temperature becomes higher (Argyle and Bartholomew, 2001).

Sintering is a complicated process, in physical and chemical nature. It depends on parameters affecting catalytic technologies including time, temperature, atmosphere, metal species and support material. In general, it is preferable to inhibit or postpone it rather than to reverse it. Since sintering is strongly dependent on temperature, decreasing the temperature is the most direct approach to reduce the rate of sintering (Adibi, 2014).

2.1.4 Other Mechanisms of Deactivation

Other than the three main mechanisms mentioned above, the performance of catalyst can be affected by other mechanisms such as masking or pore blockage. These mechanisms occur when the outer surface of catalyst is physically deposited by other substances thereby blocking the access of reactants to the active sites. Apart from the coke deposition discussed in the previous section, masking takes place when the catalyst external surface is attached by metals present in feed. It can be seen in the hydrotreating processes (Forzatti and Lietti, 1999).

Moreover, certain catalyst may lose the active phase by vapour transport. Since the temperatures for metals to be vaporized are very high, catalyst is generally not caused by the direct volatilization of the metals in most of the catalytic processes. In contrast, volatile compounds are formed with the loss of metals at moderate temperatures in some catalytic reactions. Table 2.3 lists down the types of volatile compounds that may be formed, including metal carbonyls, oxides, sulphides and halides. According to Bartholomew (2006), by testing of Pd-Ru catalyst in an automobile exhaust converter for a period of time, Ru was found to have a significant loss due to the formation of volatile RuO_x (Bartholomew and Farrauto, 2006).

Table 2.3: Possible volatile metal compounds generated in catalytic processes. (Bartholomew and Farrauto, 2006)

Gaseous Environment	Type of Compound	Example
CO, NO	Carbonyls, Nitrosyl carbonyls	$\text{Ni}(\text{CO})_4$, $\text{Fe}(\text{CO})_5$
O_2	Oxides	RuO_3 , PbO
H_2S	Sulphides	MoS_2
Halogens	Halides	PdBr_2 , PtF_6

Depending on the types of reactor used, mechanical deactivation of catalyst can occur in different forms, including crushing due to load, attrition and erosion caused by high fluid velocity. Attrition is a common problem that will be encountered in fluidized or slurry bed. The attrited catalyst particles will become smaller in size or be rounded or smoothened. On the other hand, crushing of catalyst particles may take place in fixed bed reactors (Bartholomew, 2001).

Catalysts are generally prepared by agglomeration of particles which are assembly of primary particles and then followed by processes like extrusion and compaction. The catalysts formed are considered to have lower strength than those smaller particles and thus are easier to occur mechanical failure (Argyle and Bartholomew, 2015). A catalyst with better mechanical strength is desirable as it is more resistant against crushing and attrition. When the catalyst has poor resistance to crushing or attrition, significant pressure drop or shut down of certain units may happen in catalytic processes.

Mechanical failure of catalyst can occur through two mechanisms: (i) fracture of catalyst particles into much smaller size and (ii) erosion from catalyst surface. Catalysts will experience various stresses during their life cycle. The former case may be caused by mechanical, thermal or chemical stresses while the latter one is due to mechanical stresses. There are mechanical stresses when the catalyst particles collide with each other as well as with reactor walls. Also, a fluid at high velocity may form turbulent eddies or collapsing bubbles and result in shear forces. In the matter of thermal stresses, catalyst particles will expand when being heated up whereas the opposite will occur when they are being cooled down. Thermal stresses are greatly dependent on the temperature gradient across the catalyst particles and the thermal expansion coefficient of the material. Lastly, chemical stresses arise when there are phases having differences in density are formed through chemical reaction in the catalyst particle (Bartholomew and Farrauto, 2006).

2.2 Ostwald Ripening

In 1896, Wilhelm Ostwald first qualitatively described the phenomenon in which inhomogeneous structure evolves over time as Ostwald ripening. It can be observed in both solid and liquid solutions. As already mentioned above, Ostwald Ripening, also known as atomic migration, is one of the mechanisms of catalyst sintering. Since the focus of this study is on Ostwald ripening, this topic will be reviewed extensively.

2.2.1 Thermodynamic Driving Force for Ostwald ripening

For the case of supported metal particles, the Gibbs free energy is expressed as follows:

$$dG = \mu_0 dN + \sigma_M dA + \sigma_S dA_S + \sigma_{MS} dA_{MS} \quad (2.4)$$

where μ_0 refers to the chemical potential of bulk material, A refers to the metal particle free surface area, A_S and A_{MS} are area of support and metal-support interface respectively, and σ_M , σ_S and σ_{MS} represent the surface energy of metal particle, support and metal-support interface respectively. The energy of a metal particle is affected by (Berg, 2016):

- (1) the amount of surface energies contributed for total energy
- (2) the surface energies of both metal and support which may be affected by reaction conditions
- (3) the interaction of metal and support which may differ according to the chemical nature of support
- (4) the metal-support interfacial area which is dependent on surface energy as well as the support structure (eg: size and shape)

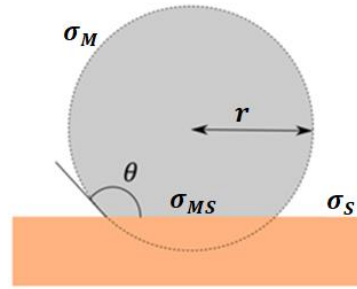


Figure 2.8: Schematic illustration of a particle on flat surface
(Berg, 2016)

The area of metal-support interface increases as the surface area of support diminishes. The formation of metal-support interface also depends on the ability of particles to maintain contact with support surface. The relationship between the three surface energies (σ_M , σ_S and σ_{MS}) can be expressed as Young-Duprez relation:

$$\sigma_M \cos(\theta) = \sigma_S - \sigma_{MS} \quad (2.5)$$

where θ is the angle between particle surface and the outline of support surface (Berg, 2016). By considering the chemical potential of metal nanoparticles, the equation becomes

$$\mu = \left(\frac{\partial G}{\partial N} \right) = \mu_0 + \frac{2\sigma_M V_m}{r} \quad (2.6)$$

where V_m is the volume of an atom in the nanoparticle and r is the radius of metal nanoparticle (Berg, 2016). This equation is known as Gibbs-Thomson relation. As predicted from Gibbs-Thomson relation, the chemical potential of particles is inversely proportional to their size especially for those with small radius.

For the sake of minimum Gibbs free energy, the system will always try to achieve minimum surface area. When there are particles in different sizes, the systems will be driven by the gradient in chemical potential to reach a state of lower energy. The chemical potential is large at smaller particles as compared to larger

particles. The studies of Ratke and Voorhees (2011) and Campbell *et al.* (2002) showed that particles which are smaller in size are less energetically stable than those relatively larger particles. Due to smaller ratio of surface area to volume, larger particles have lower surface free energy and thus present in lower energy state. Besides that, in contrary to the molecules on the particle surface, molecules which are well and orderly packed in the interior of the particles are more energetically stable. In order to reduce the overall energy, molecules or atoms of small particles especially those on surface are prone to escape and diffuse across the support surface or the solution, and finally deposit on the surface of larger particles. As a consequence, the larger particles continue to grow in size with the shrinkage of smaller particles until they are lost in the system. In the meantime, the volume fraction of coarsening particle (ϕ) remains constant with time (Werz *et al.*, 2014).

In other words, the concentration of molecules is larger near the surface of smaller particles than around large particles. In respect to the concentration gradient, a net diffusive flux of atomic species from small particles to comparatively large particles will be induced, thereby resulting in the growth of large particles accomplished with the expense of small particles (Simonsen *et al.*, 2011). Thus, in addition to the increase in average size of particles, the number of particles declines over time.

As shown in Figure 2.9, the diffusion of particles can occur through the reaction medium in liquid or vapour phase as well as through the support surface. In the former case, the reaction medium is the main parameter causing the difference in diffusion coefficient of metal particle whereas for the latter case, the diffusion coefficient of metal particle is related to its interaction with support. Therefore, Ostwald ripening may be either reaction-limited or diffusion-limited (Berg, 2016).

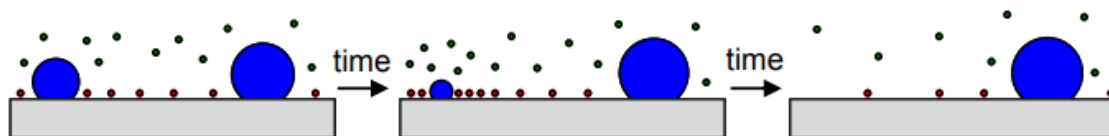


Figure 2.9: Illustration of particle growth via Ostwald ripening. Metal particle is represented by blue color while the support is shown in grey. Metal atoms diffusing through reaction medium and support surface are in green and red respectively. (Berg, 2016)

2.2.2 Theory of Ostwald Ripening

The theory of Ostwald ripening describes the evolution of particles over time. The classical theory of Ostwald ripening was developed by Lifshitz and Slyozov (1961), and Wagner (1961). Nowadays, this theory is referred as LSW theory. The important quantities in this theory include the function of particle distribution $f(r, t)$, the average particle radius $r(t)$, and the total number of particles $N(t)$. The LSW theory can be applied only in the case which the volume fraction of the coarsening phase approaches to zero ($\phi \rightarrow 0$) (Yao *et al.*, 1993). LSW theory was developed based on the assumptions as shown hereunder (Viswanatha and Sarma, 2007):

- (1) The particles are spherical in shape and grow in a supersaturated medium;
- (2) The growth or shrinkage of particles is only related to the infinite mean field concentration;
- (3) The total mass of the solute is conserved;
- (4) The particle size distribution can only be characterized in terms of radius distribution continuous function, valid in the limit of a sufficiently larger number of particles in the system to justify such a continuum description;
- (5) Processes that introduce new particles, for example, nucleation and aggregation, are negligible.

Based on these assumptions, an asymptotic solution is obtained. Since the solubility of particles is directly correlated to their size, there should be a critical particle radius, R^* , at which when the radius of the particle is found to be equal to the critical radius, it will not grow or dissolve. That means that the growth or shrink rate of the particle is zero. When the particle is larger than the critical radius ($r > R^*$), it will grow. Alternatively, when the particle is smaller than critical radius ($r < R^*$), it will dissolve or shrink in size (Balcan, 2002). In the asymptotic limit, the correlation between the average particle radius and the critical particle radius described as r/R^* is a constant. Apart from that, there are three equations which are kinetic, continuity and mass conversion equation are required in the LSW theory. Kinetic and continuity equation describe the growth or diminishing of a given size particle and the evolution of a particle size distribution with time, respectively. Among these equations, the mass conservation of the solute is dependent on the asymptotic solution of the kinetic and continuity equation. As a result, the asymptotic state of the system is not dependent on the initial conditions (Rao, Muller and Cheetham, 2006). In the review on LSW theory, the evolution of particle radius distribution related to time can be given as the equation below:

$$f(r, t) = \kappa \xi^2 \left(\frac{3}{3+\xi} \right)^{7/3} \left(\frac{1.5}{1.5-\xi} \right)^{11/3} \exp \left(\frac{-\xi}{1.5-\xi} \right) \quad (2.7)$$

$$\xi = \frac{r}{\bar{r}} \quad (2.8)$$

$$\kappa = \frac{\kappa_c}{(1+t/\tau_D)^{4/3}} \quad (2.9)$$

$$\tau_D = \frac{9\bar{r}_0^3 RT}{64\sigma D C_\infty V_m^2} \quad (2.10)$$

where r represents the radius of particles and \bar{r} represents the average particles radius. κ is related to time t by Equation 2.9 where τ_D is the time constant given by Equation 2.10. \bar{r}_0 represents the average particle radius at $t = 0$ and D is diffusion coefficient of the system. Besides that, by integrating Equation 2.7, an expression for the average particle radius at time t can be obtained:

$$\bar{r}^3 - \bar{r}_0^3 = Kt \quad (2.11)$$

where K can be expressed by $K = 8\sigma DV_m^2 C_\infty / 9RT$.

Figure 2.10 below shows the standard form of $f(r, t)$ where the function appears as asymmetric curve when the particle diameter is large. It is being cut off at the radius r which is around 1.3 to 1.5 times of the average radius \bar{r} (Hansen *et al.*, 2013).

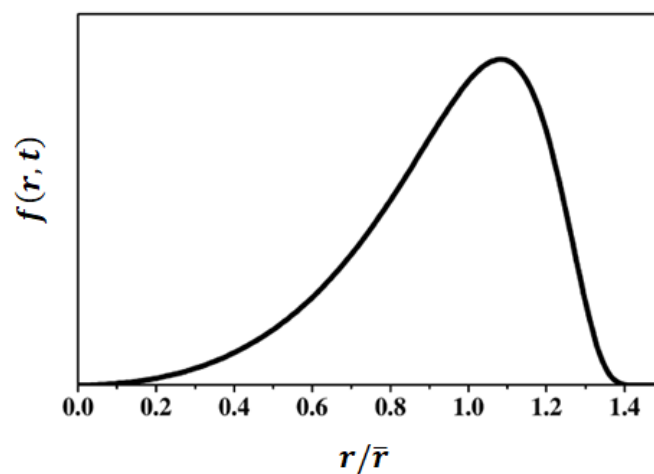


Figure 2.10: Typical line shape of particle size distribution based on LSW Theory. (Rao, Muller and Cheetham, 2006)

In general, most of the experimental results have a broader and more symmetric distribution than what is predicted by LSW theory. The main problem with the LSW theory is that the particle growth rate is assumed to be independent to its surroundings by the mean field of kinetic equation. For example, a particle will grow with identical rate no matter the size of the surrounding particles is larger or smaller than itself (Baldan, 2002). Volume fraction (ϕ) is the proportion of the volume of the coarsening particles to the total volume of the system (Rao, Muller and Cheetham, 2006). In LSW theory, the volume fraction of the coarsening particles is considered to be very small. However, there is a large difference between the specified and realistic value of ϕ , leading to the error between experimental and theoretical particle size distribution. The diffusional interaction between the particles

and surroundings is one of the factors which cause these errors. Consequently, the LSW theory which is only valid for volume fraction approaching zero is difficult to be tested precisely by experiments or numerical methods. In general, experiments take into account the volume fraction larger than zero.

In order to improve the theory of Ostwald ripening, many groups addressed the limitations of LSW theory and have proposed some models which are more realistic for Ostwald ripening process by considering finite volume fraction of coarsening particles. Among a variety of groups, the more important and famous ones are Brailsford and Wynblatt (1979), Voorhes and Glickman (1983), Marqusee and Rose (1984), and Tokuyama and Kawasaki (1984). The models they developed are the BW theory, the VG theory, the MR theory and the TK theory, respectively. According to these theories, the particle size distribution function broadened quickly when the volume fraction shows a rise. The rate constant K is found to be dependent on volume fraction. At relatively small value of ϕ , the value of K climbs up significantly whereas it increases slightly once ϕ reaches a higher value (Baldan, 2002).

2.2.3 Factors Affecting Ostwald Ripening

The information on parameters which act as significant role in affecting the rate of Ostwald ripening is provided and discussed in this section. The rate of particle growth via Ostwald ripening has great correlation with various parameters including temperature, atmosphere, metal type, support porosity and the presence of promoters and impurities (Argyle and Bartholomew, 2015). It should be understood that these parameters are not individual effects, oppositely they are reciprocally connected. For example, the shape of the metal nanoparticles may be affected by the support material. That is, it is difficult to treat each of the elements as an individual role which is irrelevant to each other.

(1) Temperature

The rate of particle growth by either particle migration or Ostwald ripening is exponentially dependent on temperature and it can be expressed by Arrhenius equation (Adibi, 2014).

$$k = A \exp\left(-\frac{E_a}{RT}\right) \quad (2.12)$$

where A represents frequency factor, E_a is activation energy in J/mol, R is universal gas constant (J/mol·K) and T is temperature (K). In order for atoms or molecules on particle surface to dissociate and diffuse over the support surface, a minimum energy barrier should be overcome and this can be achieved by the change in temperature. In general, this is relevant to the absolute melting point (T_m) of the metal material. Other than that, there are another two temperatures which are Huttig temperature and Tamman temperature should be considered in this case. The Huttig and Tamman temperature are defined to be equal to $0.3 T_m$ and $0.5 T_m$, respectively. As temperature increases to Huttig temperature, the atoms on surface are readily active to detach and diffuse. By further increasing the temperature to reach Tamman temperature, atoms are observed to be more mobile. What it means is that the sintering of supported metal nanoparticles is initiated at Huttig temperature while its rate is increasing with increase of temperature to Tamman temperature. In the case of methanol synthesis with the presence of copper catalyst, the copper particles are found to start to grow at temperature around 463 to 500 K and the rate increases obviously at 543 to 573 K (Basile and Dalena, 2017).

(2) Atmosphere

Gas environment is also a principal factor in affecting the sintering rate of particles. The sintering rate of noble metals is found to be more rapid in oxygen than in hydrogen. In the case of Pt catalyst, its sintering rate is

reported to decrease progressively in the sequence of $\text{NO} > \text{O}_2 > \text{H}_2 > \text{N}_2$ (Argyle and Bartholomew, 2015).

The sintering rate is related to the ability of an atom to get free from a particle as well as to diffuse over the support surface. However, these values will be affected. The reason is that, by changing the gas environment, the character of the particles and the interaction between the metal particles and support will be changed. In oxidizing environment, metal complexes such as PtO_x may be formed. In comparison to metal adatom, these species may have different detachment rate from particle to surface. Other than that, the surface velocity will also be different. When the dissociation activation energy or surface velocity is lower, the concentration of migrating surface atoms will increase (Flynn and Wanke, 1974). Additionally, the properties of support such as structure and chemical state will also be influenced by the atmosphere which in turns affects particles stability (Adibi, 2014).

(3) Type of Metal and Support

Since the thermal stability of metal particles varies in different atmosphere, type of metal to be used in catalytic process is important. In reducing atmosphere, oxygen and other oxidizing compounds are removed while the reducing agents such as hydrogen as well as compounds that will be oxidized if any oxygen presents, for example hydrogen sulphide are remained. In such condition, the stability of metal is directly proportional to the melting temperature. As such, the metal stability decreases as $\text{Ru} > \text{Ir} > \text{Rh} > \text{Pt} > \text{Pd} > \text{Ni} > \text{Cu} > \text{Ag}$. On the other hand, for metal in oxidizing environment, the stability should consider the volatility of metal oxides and the interaction between metal oxide and support. In air, the stability of noble metals reduces in the following sequence: $\text{Rh} > \text{Pt} > \text{Ir} > \text{Ru}$. The reason that ruthenium is relatively instable is that it will form RuO_4 which is volatile (Argyle and Bartholomew, 2015).

These orders may be changed due to interactions between metal and support. For example, in vacuum, the thermal stability of Pt on different support from high to low is $\text{Pt}/\text{Al}_2\text{O}_3 > \text{Pt}/\text{SiO}_2 > \text{Pt}/\text{C}$ (Argyle and Bartholomew, 2015).

(4) Promoters or Impurities and Pore Size of Support

The presence of promoter or impurities may cause the metal-support interaction to either increase or decrease. Take oxygen as an example, in many studies, oxygen is reported to greatly reduce the mobility of metal atoms on support, resulting in a decline in sintering rate. This is because a metal oxide layer will be formed on the support surface (Flynn and Wanke, 1974).

Geus (1971) pointed that the impurities on the both metal or support surface can affect particle shape and cause a rise in metal-support interaction thereby slow down sintering rate. Furthermore, due to the fact that the nucleation and growth of crystals tend to occur at defect sites, the detachment of metal atoms from particles to support surface may be restricted. Similarly, the pores on support surface will inhibit the mobility of particles on surface especially when the diameter of pores is almost identical to the size of metal particle (Argyle and Bartholomew, 2015).

(5) Metal Loading

According to Bartholomew (1993), sintering rate increases when surface particle density is higher. This can be achieved by reducing support area or increasing metal loading.

Initially, a simple power-law expression (SPLE) was used to describe sintering rate.

$$-\frac{d\left(\frac{D}{D_0}\right)}{dt} = k_s \left(\frac{D}{D_0}\right)^n \quad (2.13)$$

where k_s represents sintering rate constant, D_0 is the initial dispersion and n is the order of sintering. However, SPLE have several limitations such as it is not able to quantify or compare the data obtained from different conditions. SPLE assumes that surface area approaches to zero for a period of time. This assumption is then found to be not consistent with the fact that the surface area or dispersion will not eventually equal to zero at given conditions such as temperature and atmosphere for a certain period of time. Moreover, for a given catalyst and given atmosphere, the sintering order is found to be dependent on time and temperature (Bartholomew, 1993).

Therefore, Fuentes and Bartholomew (2001) proposed the general power law expression which can quantify the parameters affecting the sintering rate by fitting the kinetic data.

$$-\frac{d\left(\frac{D}{D_0}\right)}{dt} = k_s \left(\frac{D}{D_0} - \frac{D_{eq}}{D_0}\right)^m \quad (2.14)$$

where a term $-\frac{D_{eq}}{D_0}$ is added to consider the dispersion versus time curve to a limiting dispersion D_{eq} at infinite time. m is sintering order where reported to be 1 or 2 (Argyle and Bartholomew, 2015).

2.2.4 Examples of Catalytic Reactions with Ostwald Ripening

As Ostwald ripening is not uncommon in the industrial catalytic reactions, this topic will cover some of the examples found in the industry.

2.2.4.1 Methanol Synthesis

The main steps in methanol production can be briefly described as:

- (1) Preparation of syngas
- (2) methanol synthesis
- (3) purification of methanol

In the review by Basile and Dalena (2017), the operating conditions for methanol production conducted in vapour phase are typically carried out at temperature of 200 °C to 300 °C and pressure ranging from 50 to 100 atm. In this process, copper-based catalyst which is made up of CuO, ZnO and Al₂O₃ is used. The composition of each catalyst can differ according to different manufacturer. In CuO/ZnO/Al₂O₃ catalyst, metallic copper acts as main active metal while ZnO and Al₂O₃ have been reported to be support and promoter respectively. Additives such as promoter or stabilizer can also be applied. In this case, MgO is added, leading to lower operating temperature and slower sintering.

Copper-based catalyst is revealed to be advantageous with regard to activity and selectivity. However, it is not used before 1960s in large scale due to its poor stability. This may due to the presence of sulphur species in syngas. Consequently, syngas should be deeply purified before reaction in order to largely decrease the occurrence of sulphur poisoning. Catalyst deactivation occurs in methanol synthesis and decreases the active surface area, resulting in shorten catalyst lifetime. As mentioned before, there are several types of catalyst deactivation mechanisms including coking and sintering. In the case of methanol synthesis, only small amount of methane and C²⁺ molecules will be formed. The reason is that the copper particles are not sufficient to either form C-C bond or break the C-O bond in CO and CO₂. Therefore, the catalyst deactivation resulted by fouling or coking is inconsequential. If the concentration of CO₂ in feed is high and that of CO and CO₂ are low, the catalyst deactivation may take place as oxidation. These deactivations may occur for the first few hours of operation but not for longer time since they are expected to keep in equilibrium after a certain period of time (Berg, 2016).

After all, the main mechanism that contributes to the deactivation in methanol synthesis is reported to be the sintering of copper particles. According to Berg (2016), Ostwald ripening is the dominant mechanism in causing the catalyst deactivation in methanol synthesis. The catalyst performance is dependent on the total area of copper exposed in the system. Therefore, the ratio of surface area to volume is better to be high in order to achieve higher activity. What it means in practice is that the size of copper particles should be small. However, small size particles result in high ratio of surface area to volume. For this reason, particles

which are smaller in size are less energetically stable than those relatively larger particles, resulting in a tendency for particle growth. In methanol synthesis, due to the presence of ZnO and Al₂O₃, the copper particles are physically separated and thus will not collide with each other directly. Alternatively, the particles grow via particle migration or Ostwald ripening. As the copper particles strongly attach on supports, the particles prefer to diffuse across the support surface rather than to dissociate from support surface. The concentration of copper particles is larger near the smaller one and thus less stable. A net diffusive flux of copper atomic species from smaller particles to larger ones occurs as a result of difference in concentration. Thus, the larger particles become bigger at the expense of smaller ones.

2.2.4.2 Fischer-Tropsch Synthesis (FTS)

Fischer-Tropsch synthesis (FTS) is a catalytic process which converts synthesis gas (CO and H₂) into liquid hydrocarbons. Transition metals cobalt and iron are the metals commonly used in industrial scale. In several studies, FTS catalysed with cobalt has been reported to experience catalyst deactivation. For instance, the review by Saib *et al.* (2006) provided that several deactivation mechanisms including coking and sintering occur on Co/Pt/Al₂O₃ concurrently during FTS while on different timescales.

In a study of Kistamurthy *et al.* (2015), FTS with a planar model catalyst where SiO₂(100) single crystal is deposited by Co has been studied to investigate the mechanisms of sintering. By using planar model catalyst, the loss of active surface sites can be inspected at single-particle level. In their study, the model catalyst Co/SiO₂ was exposed to low conversion FTS conditions using 20 bar dry and pure synthesis gas (H₂/CO: 2/1) at temperature of 230 °C for a period of 10 h. Catalyst characterization was carried out to obtain the physical and chemical characteristics of the model catalyst before and after exposed to the FTS conditions. Figure 2.11 shows the transmission electron microscopy (TEM) images of the same area on the model catalyst before (Figure 2.11a) and after (Figure 2.11b) the exposure to FTS condition.

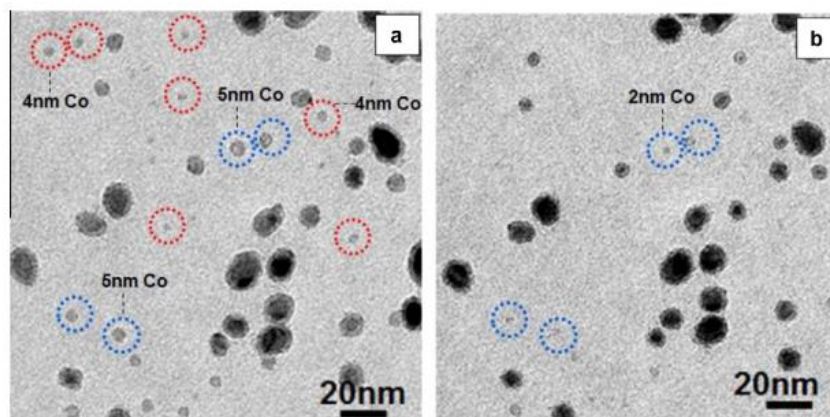


Figure 2.11: TEM images of the same area on the model catalyst Co/SiO₂ before (a) and after (b) the exposure to FTS condition. Blue circles indicate the particles which have shown significant decrease in size during FTS while red circles indicate the particles which have disappeared during FTS (Kistamurthy *et al.*, 2015).

In comparing between both of these images, some of the smaller Co particles are found to eventually disappear while some particles decrease significantly in size during the FTS. The growth of Co particles through the migration of entire particles followed by the collision and coalescence of particles is not observed on the model catalyst exposed to the FTS conditions by the TEM. Therefore, the loss of catalyst active sites due to the diffusion of Co atoms emitted by smaller Co particles over the support surface reveals that Ostwald ripening is the dominant sintering mechanism for the model catalyst under the FTS conditions used. Since this happens in a 10 h time interval which is relatively short, the reduction of active surface area is considered as a rapid process which occurs in the early stage of FTS (Kistamurthy *et al.*, 2015).

Apart from that, the review by Hansen *et al.* (2013) also provided a similar mechanism for sintering of Ni on MgAl₂O₄ under a reaction condition of 0.004 bar H₂/H₂O (1:1) at temperature of 750 °C. In this study, the loss of small Ni particles is observed in the early stage of the process. As a result, the sintering of Ni is deduced to be caused by Ostwald ripening rather than particle migration.

2.3 Hydrogenation Reaction

Hydrogenation is a chemical reaction between hydrogen and other compounds which normally involves the use of bulk metal catalyst such as nickel, lead and platinum or supported metal catalysts. The process usually aims to reduce or saturate unsaturated (double bonds) organic compounds, but in some case, hydrogenation is used to transform from a species to another, for example in the case of citral. Many studies have been carried out to study the factors affecting the activity of hydrogenation catalysts. Based on several researches, Hastert (1979) has concluded the different parameters that can affect the rate of catalytic hydrogenation, for example, temperature, pressure and catalyst loading. The following subtopics review the type of reactants that will be used for hydrogenation in this study.

2.3.1 Fats and Fatty Acids

Fats and oils are made up of fatty acids and glycerol where fatty acids are long hydrocarbon chain linked with carboxyl groups. Fatty acids have varying chain length based on the number of carbons in the chain. Fatty acids can be grouped into saturated and unsaturated by the presence of double bonds in their molecular structure. Unsaturated fatty acids contain one or more double bonds while saturated fatty acids do not have double bond in their chains. Iodine value (IV) is expressed as the mass of iodine consumed by every 100g of fats. It is commonly used to represent the extent of unsaturation of fats. Fats with lower degree of unsaturation have lower IV.

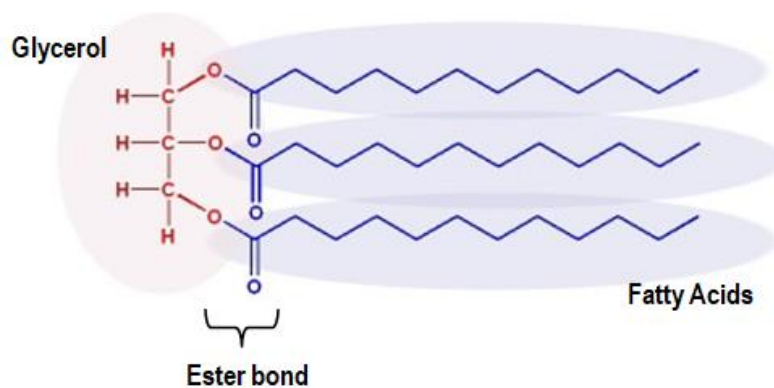


Figure 2.12: Structure of Fats

Table 2.4 and Table 2.5 show the major saturated and unsaturated fatty acids with their respective number of carbons, respectively. Number of carbon double bond in the molecular structure of fatty acids affects the physical properties such as melting point and crystallinity. Generally, the melting point of fatty acids is inversely proportional to the number of double bonds. The melting point is lower with higher number of double bonds. Therefore, fats and oils which are rich in unsaturated fatty acids exist as liquid at room temperature while ones with mostly saturated fatty acids are in solid or semi-solid forms. For example, olive oil containing mostly unsaturated fatty acids exists as liquid at room temperature while butter is solid at room temperature because it contains mostly saturated fatty acids.

Table 2.4: Major Saturated Fatty Acids (Nikita, n.d.)

Name	Number of Carbon	Abbreviation	Typical Source
Butyric Acid	4	C4:0	Butter
Caproic Acid	6	C6:0	Butter, Palm oil, Coconut oil
Caprylic Acid	8	C8:0	Palm oil, Coconut oil
Capric Acid	10	C10:0	Palm oil, Coconut oil
Lauric Acid	12	C12:0	Plants of lauraceae, Coconut oil, Palm oil
Myristic Acid	14	C14:0	Seed fats of mace, Butter, Coconut oil
Palmitic Acid	16	C16:0	Plant fats, Palm oil, Peanut oil
Stearic Acid	18	C18:0	Plant and animal fats
Arachidic Acid	20	C20:0	Peanut oil
Behenic Acid	22	C22:0	Plant lipids
Lignoceric Acid	24	C24:0	Plant lipids
Cerotic Acid	26	C26:0	Beewax, Wool

Table 2.5: Major Unsaturated Fatty Acids (Nikita, n.d.)

Name	Number of Carbon	Abbreviation	Typical Source
Palmitoleic Acid	16	C16:1	Sardine oil
Oleic Acid	18	C18:1	Olive oil, Peanut oil, Linseed oil
Linoleic Acid	18	C18:2	Olive oil, Peanut oil, Linseed oil, Soybean oil
Linolenic Acid	18	C18:3	Linseed oil
Parinaric Acid	18	C18:4	Plant lipids
Erucic Acid	22	C22:1	Rapeseed oil
Arachidonic Acid	20	C20:4	Peanut oil

Saturated fatty acids can be found in fats and oils and can also be formed by hydrogenation of unsaturated fatty acids. During hydrogenation process, hydrogen atoms are added into the double bonds of unsaturated fatty acids hence lessens the number of double bonds. It can be seen from the hydrogenation of oleic acid shown in the Figure 2.13. By complete hydrogenation, all the unsaturated fatty acids may be converted into saturated ones having the same carbon number. As presented in Figure 2.14, linolenic acid is eventually converted into stearic acid after a complete hydrogenation.

**Figure 2.13: Hydrogenation of Oleic Acid (Ophardt, 2003)**

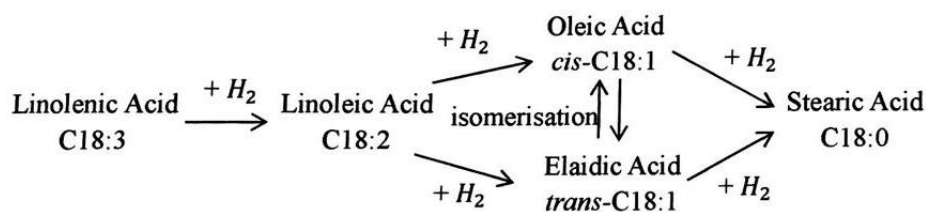


Figure 2.14: General Hydrogenation Scheme of Linolenic Acid

Upon hydrogenation, the melting point, solid content and oxidative stability of the fats are increased without affecting their carboxyl functionality (Gutsche, 2008). Unsaturated fatty acids show a tendency to turn rancid due to the reaction between the reactive double bonds in unsaturated fatty acids and oxygen in air. The rancidity of fatty acids may also occur by exposure to heat. By reducing the number of double bonds, the stability of fatty acids during exposure to air and heat is improved (Bartholomew *et al.*, 2006).

2.3.1.1 Crude Palm Oil (CPO)

Crude palm oil (CPO) is an edible oil which is extracted from the mesocarp of oil palm fruit. CPO is different from palm kernel oil (PKO) or coconut oil where PKO is extracted from the kernel or seed of the fruit. Even though both of them originate from the same fruit, they have large difference in composition, density and appearance. CPO exists naturally as semi solid at room temperature with deep orange red colour due to high content of natural carotenes. CPO contains high amount of carotenoids, tocopherols and tocotrienols (vitamin E) which provides natural stability against oxidative deterioration (Gibon, Greyt and Kellens, 2007). In general, CPO contains balance ratio of 50 % saturated fatty acids, 40 % of monounsaturated fatty acids and 10 % polysaturated fatty acids (MPOC, n.d.). The major saturated fatty acids in CPO are palmitic acid (C16:0) and stearic acid (C18:0) while the main unsaturated fatty acids in CPO are oleic acid (C18:1) with single double bond and linoleic acid (C18:2) with two double bonds.

CPO usually undergoes refining which is a process of purification prior to further application to remove the undesired minor constituents in the oil without damaging the acylglycerols and causing loss in desirable constituents (Gibon, Greyt and Kellens, 2007). As shown in Figure 2.15, there are two methods to conduct the refining process which are known as physical refining and chemical refining (Shahidi, 2005).

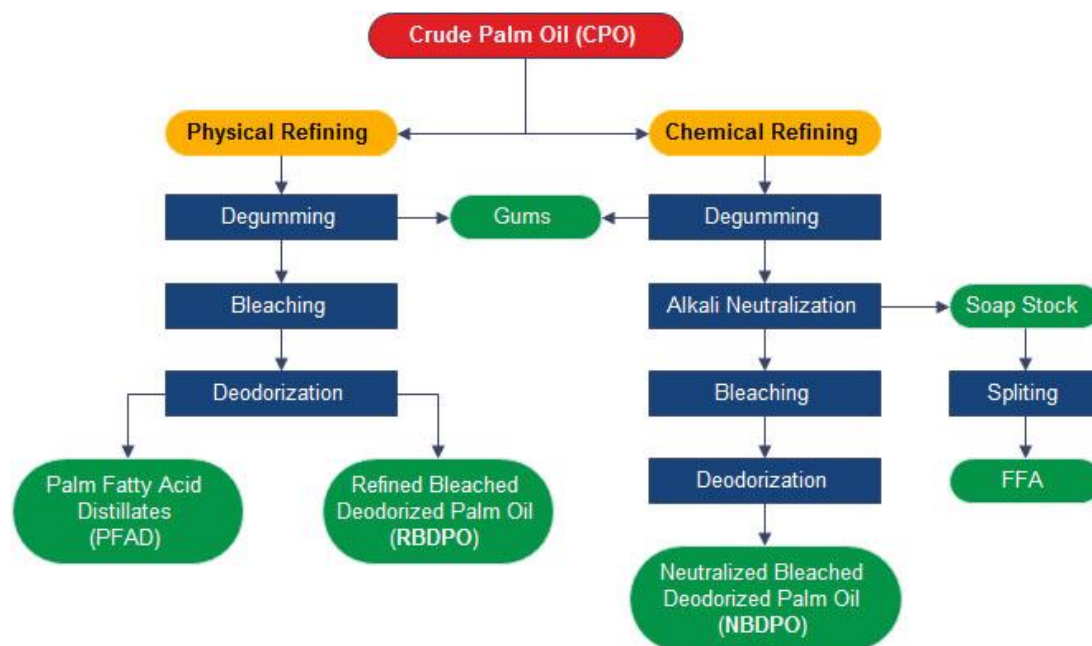


Figure 2.15: Refining process for crude palm oil (CPO)

Table 2.6: Refining process for crude palm oil (CPO) (Shahidi, 2005)

Process	Application
Degumming	Removal of free fatty acids by adding concentrated phosphoric acid
Bleaching	Removal of main particles of color bodies, metal contamination and oxidizing materials in the oil
Deodorization	Removal of free fatty acids and undesired odor and taste substances from the oil.

After undergoing refining process, the product obtained is refined, bleached and deodorized oil (RBDPO) in light orange colour. RBDPO is commonly used for production of many food products, for example, margarine, ice cream, chocolate and bakery products. Other than that, RBDPO is also widely used in non-food products including soap, candles and cosmetics.

2.3.1.2 Lauric Acid

Lauric acid, also known as dedecanoic acid, is a 12-carbon medium chain saturated fatty acid. At room temperature, lauric acid exhibits as white solid with low melting point of 40 to 44 °C (Ezigbo and Mbaegbu, 2016). It makes up almost half of the fatty acids within palm kernel oil or coconut oil. Palm kernel oil and coconut oil are necessary to go through the refining process as mentioned in the previous section to remove impurities that are not fit to be consumed. With large amount of saturated fatty acids, palm kernel oil and coconut oil yield harder fat when fully hydrogenated

Besides that, lauric acid can be found in human or animal body where it is converted into monolaurin which is more functional. Monolaurin is found to be an antiviral antibacterial and antiprotozoa monoglyceride having capability of destroying viruses including HIV, herpes and other pathogenic bacteria (Ezigbo and Mbaegbu, 2016). Apart from being use as medicine, lauric acid is widely used in production of beauty products, skin care products, soaps and shampoo due to its moisturizing ability.

2.3.1.3 Splitted Palm Stearin Fatty Acids (SPSFA)

Splitted palm stearin fatty acids are obtained by fractionation and splitting of palm oil (RBDPO) after crystallization at certain temperature. Palm oil is made up of substantial quantities of both low and high melting point triglyceride and thus is readily to be crystallized by controlled cooling and separated into low melting fraction olein triglycerides and high melting fraction stearin triglycerides (Deffense,

1985). In order to obtain splitted palm stearin fatty acids, the high melting fraction stearin triglycerides are subjected to splitting or so called hydrolysis process with reaction as shown in Figure 2.16. The acidity of fats is dependent on the quantity of free fatty acids present. Therefore, SPSFA consisting of high level of free fatty acids is more acidic as compared to other fats samples (CPO and lauric acid).

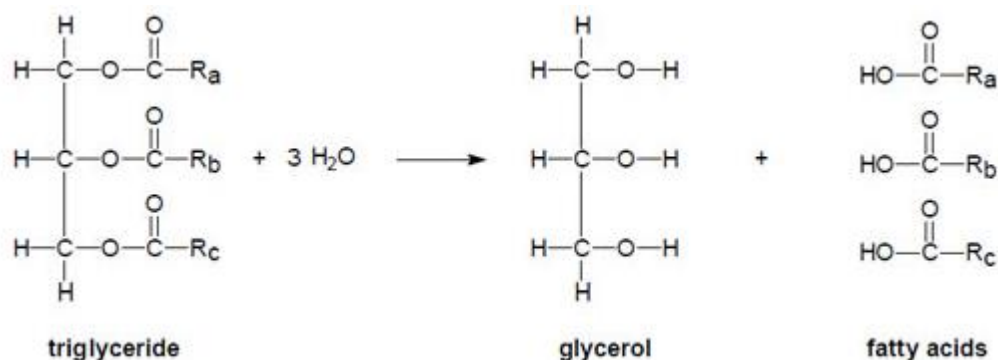


Figure 2.16: Reaction schematic of fat splitting process

2.3.2 Citral

Citral, also called 3,7-dimethyl-2,6-octadienal, is α, β -unsaturated aldehyde with molecular formula of $\text{C}_{10}\text{H}_{16}\text{O}$. It exists as pale yellow liquid with a strong lemon odor which present in the essential oils of several plants. It is insoluble in water but soluble in organic compounds including ethanol, diethyl ether. Chemically, citral is an isomeric mixture of neral and geranial which are aldehydes having same molecular formula but in different structures (Aumoet *al.*, 2005). Figure 2.17 presents the structure of neral and geranial.

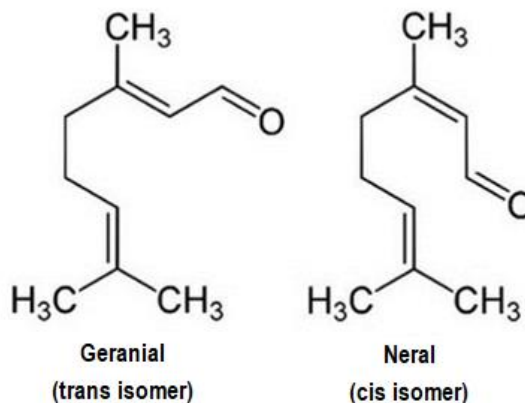


Figure 2.17: Structure of Geranial and Neral

Since citral is an unsaturated aldehyde, it is of great interest for hydrogenation from both scientific and industrial points of view. Citral has three sites available for hydrogenation which are the conjugate double carbon bond (C=C), the carbonyl group (C=O) and the isolated carbon double bond (C=C) (Hassan, 2013). The possible reaction pathways, intermediates and products during hydrogenation of citral are presented in Figure 2.18.

Unsaturated alcohols, nerol and geraniol (3,7-dimethyl-2,6-octadien-1-ol) with molecular formula of $C_{10}H_{18}O$, can be obtained from the hydrogenation of C=O bond (Hassan, 2013). Nerol and geraniol are the most valuable products from citral hydrogenation as they are involved in wide range of commercial uses, including flavours, cosmetics, perfumes, personal care products and insect repellents. Hydrogenation of the conjugated C=C bond forms citronellal ($C_{10}H_{18}O$ and 3,7-dimethyl-6-octenal). Hydrogenation of citronellal C=C bond or hydrogenation of nerol and geraniol C=O bond can lead to citronellol ($C_{10}H_{20}O$ and 3,7-dimethyl-6-octen-1-ol) (Hassan, 2013). Both citronellal and citronellol are employed in the production of detergents, soaps and perfumes due to their highly pleasant odors. 3,7-dimethyl-octanal can be produced from the hydrogenation of isolated C=C bond (Hassan, 2013). It is an undesired compound as it causes an unpleasant smell to the products mixture. Apart from the main reaction pathways mentioned above, citronellal can be converted to isopulegol through the secondary process called cyclization. Isopulegol is an intermediate during the citral hydrogenation which is

usually employed in the synthesis of methanol or formation of acetals (Bertero et al., 2009; Ekou et al., 2012).

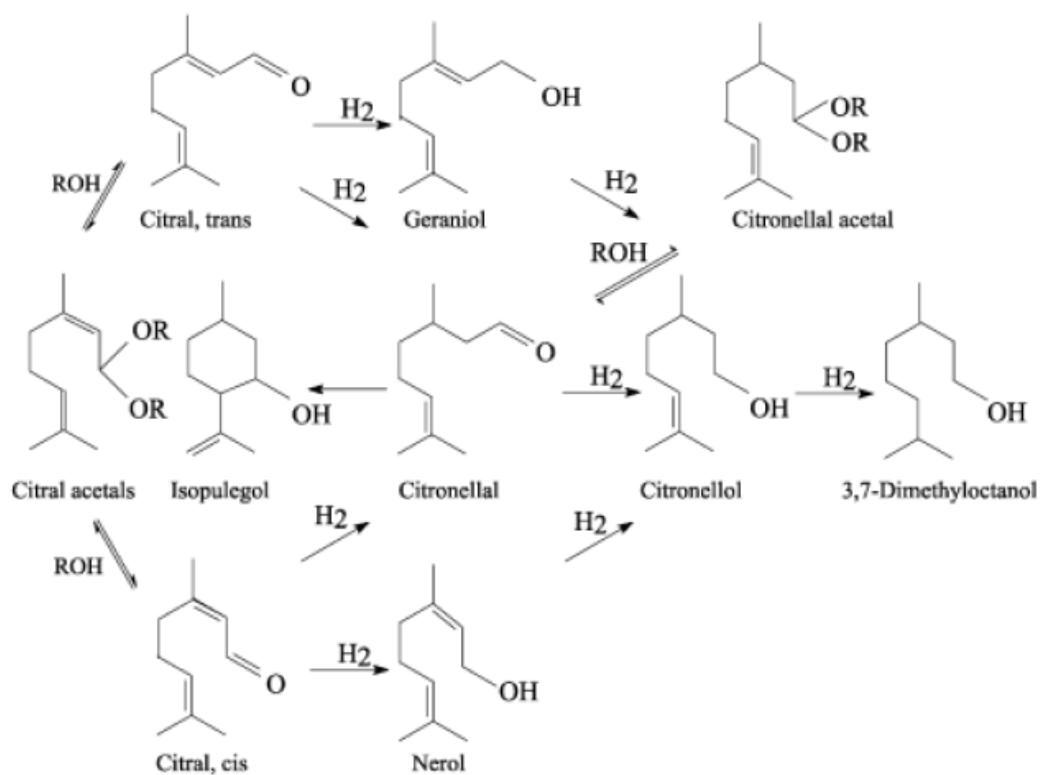


Figure 2.18: Reaction Scheme for Hydrogenation of Citral (Maki-Arvela et al. 2003)

CHAPTER 3

METHODOLOGY

3.1 Materials

In this project, the supported metal catalyst used was commercial Pricat Ni/SiO₂ in pellet form. For hydrogenation process, the organic compounds chosen were crude palm oil (CPO), lauric acid, splitted palm stearin fatty acid (SPSFA) and citral. The citral used in this project was provided by BASF (Malaysia) Sdn Bhd with composition of neral > 45 % and genranial > 45 %. Comparisons between the properties of spent catalyst during different hydrogenation processes were conducted.

3.2 Partial Hydrogenation Process

To investigate the extent of catalyst deactivation, the fresh Ni/SiO₂ catalysts were subjected to partial hydrogenation of different organic compounds (crude palm oil, splitted palm stearin fatty acid, lauric acid and citral) which was carried out in batch mode through stirred tank reactor. With every 1 L of organic sample, 2 g of catalyst was added. The reaction conditions for each hydrogenation process were tabulated in Table 3.1.

Table 3.1: Operating conditions for hydrogenation process

Operating Parameters	Operating Condition
Volume of organic compound for each reaction (mL)	500
Hydrogen Pressure (bar)	5
Temperature (°C)	195
Agitation Speed (rpm)	2000
Reaction Time (hour)	4
Mass of catalyst for each reaction (g)	1.2

The following outlined the start-up and shut down procedures involved in the hydrogenation process:

Start-up Procedure

- (1) The reactor was heated up to 85 °C.
- (2) The vacuum pump was started to create vacuum in the reactor. All valves except the vacuum pump part were ensured to be closed.
- (3) 500 mL of one of the organic compounds was poured into the reactor at 85°C and agitation speed was maintained at 2000 rpm.
- (4) The vacuum pump and the valve were turned off.
- (5) Temperature was increased to 195 °C.
- (6) Once the temperature reached 195 °C, the vacuum was started again.
- (7) Another 100 mL of chosen organic compound and 1.2 g of prepared catalyst sample were added into the reactor.
- (8) All valves were closed and hydrogen gas was supplied at pressure of 5 bar.
- (9) Hydrogenation process was started and the organic compound sample was collected from sampling port every 60 minutes for 4 hours.

Shut Down Procedure

- (1) The hydrogen supply was stopped and the hydrogen supply valve was closed.
- (2) Temperature was set to 90 °C.
- (3) Hydrogen gas was slowly released to catalytic oxidizer prior to atmosphere by switching on the hydrogen supply outlet valve.
- (4) The hydrogen supply valve was switched off while the nitrogen supply valve was switched on to supply nitrogen at 1 bar.
- (5) The remaining organic compound was purged out and fed into waste bottle once the temperature drops to 90 °C.
- (6) The nitrogen supply and nitrogen supply valve were switched off.
- (7) The vacuum pump was started to create vacuum in the reactor.
- (8) Rinse oil was poured into the reactor to wash away the remaining impurities and organic compound on the internal surface of reactor.
- (9) The vacuum pump and the valve were turned off.
- (10) Waiting for 10 to 15 minutes and switched on the nitrogen supply and respective valve. The rinse oil was then purged out from the reactor.
- (11) Once the reactor dropped to room temperature, the electric supply for the apparatus was switched off.
- (12) All the supply gases were ensured to be switched off without leakage.



Figure 3.1: Reactor for Hydrogenation Process

3.3 Spent Catalyst Collection

After the hydrogenation reaction was completed, the sample was unloaded and subjected to filtration to separate the spent catalysts out from the organic samples. The filtration was carried out in an oven with filter paper. As the collected spent catalysts were coated by residual fats, they were subjected to acetone washing followed by drying in a hot air oven. After that, the dried acetone washed catalysts were roasted in a furnace with temperature of 350 °C for 3 hours.



Figure 3.2: Dried acetone-washed spent catalysts collected from hydrogenated citral, CPO, lauric acid and SPSFA (from left to right).



Figure 3.3: Roasted acetone-washed spent catalysts collected from hydrogenated citral, CPO, lauric acid and SPSFA (from left to right).

3.4 Catalyst Performance Evaluation

Samples that show higher conversion in the shorter time implies that the catalysts have less deactivation, while catalysts with rapid deactivation will show little conversion. To study the deactivation, organic samples collected from the hydrogenation reactor were subjected to iodine value (IV) test and gas chromatography (GC) analysis to study the change of composition in different samples.

3.4.1 Iodine Value (IV) Test

Fats and oils are made up of fatty acids and glycerol where fatty acids are long hydrocarbon chain linked with carboxyl groups. Fatty acids can be categorized into saturated and unsaturated by the amount of double bonds present in the molecular structure. Unsaturated fatty acids contain one or more double bonds while fatty acids with no double bond in the chain are saturated. Iodine value (IV), the mass of iodine consumed by every 100g of fats, is commonly used to represent the extent of unsaturation of fats. Fats with lower degree of unsaturation have lower IV.

Iodine value test was performed on the hydrogenated fatty acids samples collected from the hydrogenation process according to the American Oil Chemist's Society (AOCS) Official Method Tg 1a-64. The magnitude of IV drop can reveal the severity of catalyst deactivation in each case. It can be calculated by using the equation provided below:

$$\text{Iodine Value} = \frac{(B-S) \times N \times 12.691}{\text{mass of sample added (g)}} \quad (3.1)$$

where B = volume of sodium thiosulphate used for blank (mL)

S = volume of sodium thiosulphate used for sample (mL)

N = normality of sodium thiosulphate solution (= 0.1)

The titration process was conducted with the following procedures:

- (1) The sample required was weighted and poured into a conical flask.
- (2) 20 mL of cyclohexane was added into the conical flask by using micropipette.
- (3) The conical flask was heated to 30-60 °C until the fatty acids was completely dissolved.
- (4) 10 mL of Wijs solution was added into the conical flask and dark brown colour solution was observed.
- (5) 10 mL of sodium acetate was added into the conical flask.
- (6) The conical flask was gently shaken for 3 minutes.
- (7) 10 mL of potassium iodide was added into the conical flask.
- (8) Initial reading of sodium thiosulphate was recorded.
- (9) Sodium thiosulphate was titrated into the mixture in conical flask until yellowish orange colour appeared.
- (10) 2 mL of starch was added. The mixture turned into dark blue in colour.
- (11) Sodium thiosulphate was continuously added until the mixture became colourless.
- (12) Final reading of sodium thiosulphate was recorded.
- (13) IV was calculated by performing on equation 3.1.
- (14) The steps above were repeated for other fatty acids samples.

3.4.2 Gas Chromatography (GC) Analysis

Gas chromatography (GC) analysis was conducted to measure the concentration of particular compound presents in hydrogenated organic samples. For fatty acid samples (CPO, lauric acid and SPSFA), the apparatus involved was a PerkinElmer Clarus 500 gas chromatography with a PerkinElmer COL-ELITE-2560 capillary column whom dimension is 100 m × 0.25 mm ID × 0.20 µm df. Helium was used as carrier gas with flow rate of 20 cm/s. During analysis, the oven, injector and flame ionization detector (FID) were operated at temperature of 175 °C, 210 °C and 250 °C, respectively. The samples were injected at 1 µL with a split ratio of 100:1. The

relative peak area of each compound was recorded to determine their compositions. Prior to GC analysis, the fats samples obtained from hydrogenation reactor were esterified to fatty acid methyl esters (FAME) according to the following procedures (Jham *et al.*, 1982).

- (1) 0.2 g of filtered sample was heated under reflux with 4 mL of 0.5 M potassium hydroxide in absolute methanol (KOH/MeOH) at 100 °C for 5 minutes.
- (2) 1.6 mL of aqueous hydrochloric acid in absolute methanol (HCl/MeOH, 4:1, v/v) was added into the mixture and was heated at 100 °C for 15 minutes.
- (3) The mixture was allowed to cool down.
- (4) 5 mL of deionized water and 10 mL of dichloromethane were added into the mixture.
- (5) The mixture was then poured into a separator funnel to extract the lower layer of organic solution.

As for citral before and after hydrogenation reaction, the gas chromatography analysis was conducted using Agilent Technologies 7890B gas chromatography with a Zebron ZB-Wax Plus capillary column whom dimension is 30 m × 0.25 mm ID × 0.50 µm df. During analysis, the oven, injector and flame ionization detector (FID) were operated at temperature of 210 °C, 220 °C and 280 °C, respectively. The samples were injected at 1 µL with a split ratio of 80:1. The relative peak area of each compound was recorded to determine their compositions.



Figure 3.4: Esterification of fats under reflux

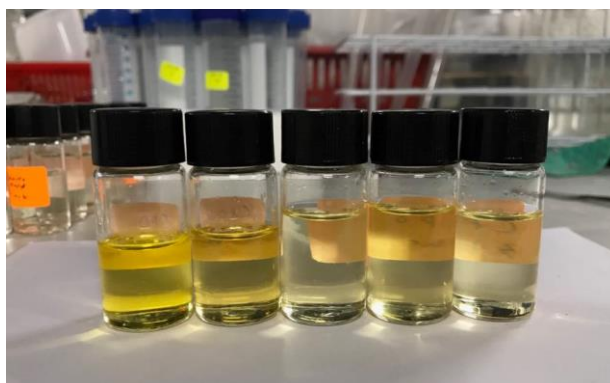


Figure 3.5: Crude palm oil (CPO) from partial hydrogenation after esterification and dissolved in dichloromethane.

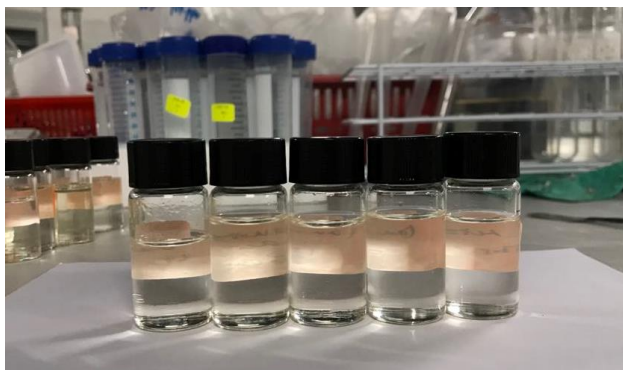


Figure 3.6: Lauric acid from partial hydrogenation after esterification and dissolved in dichloromethane.

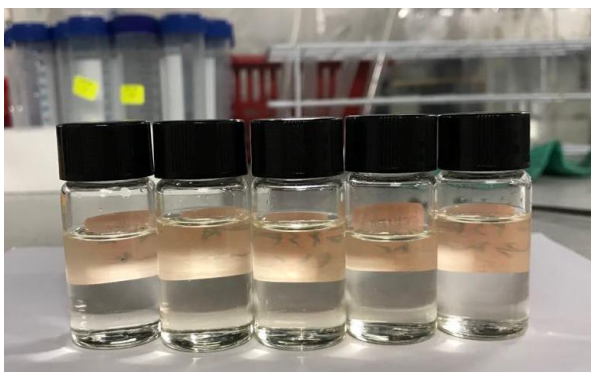


Figure 3.7: Splitted palm stearin fatty acid (SPSFA) from partial hydrogenation after esterification and dissolved in dichloromethane.



Figure 3.8: PerkinElmer Clarus 500 Gas Chromatography



Figure 3.9: Agilent Technologies 7890B Gas Chromatography

3.5 Characterization of Catalyst

Throughout the research, the physical and chemical characteristics of both fresh and spent Ni/SiO₂ catalysts, as well as their reactivity, can be analysed employing different characterization techniques and instrumentations.

For investigation of physical properties, scanning electron microscopy (SEM) was utilized. As for chemical characterization, energy dispersive X-ray spectroscopy (EDX) analysis and inductively coupled plasma optical emission spectroscopy (ICP-OES) analysis were applied.

The initial plan of the project includes the use of pulse chemisorption to study the reactivity of the catalysts by determining the dispersion and surface area of metal active sites on the catalyst surface. However, this was not carried out due to the inaccuracy of the results and limited number of slots available for results to be obtained.

3.5.1 Scanning Electron Microscopy with Energy Dispersive X-ray Spectroscopy (SEM-EDX)

Scanning electron microscopy (SEM) allows users to inspect objects under a very fine scale. It is a direct approach which provides direct images of sample surface which aids the study of the morphology and topography of the catalyst sample. A Hitachi S-3400N scanning electron microscope operated at accelerating voltage of 20kV with varying magnification was used for the measurements. A small amount of samples was placed on the multi sample holder and coated with a layer of palladium and gold with Emitech Sputter Coater to increase their conductivity. Energy dispersive X-ray spectroscopy (EDX) analysis was carried out in conjunction with SEM to study the elemental composition within the samples. The pictures and results were taken from three different spots on the samples.



Figure 3.10: Hitachi S-3400N scanning electron microscope

3.5.2 Inductively Coupled Plasma Optical Emission Spectroscopy (ICP-OES)

Inductively Coupled Plasma Optical Emission Spectroscopy (ICP-OES) is capable in detecting chemical elements with very low concentration. Nowadays, it is commonly used in determining the metal content of catalysts. According to Rouessac (2007), for ICP-OES, the energy of a high frequency generator directed to an appropriate gas which is argon in most cases leads to the formation of inductive plasma. The plasma ionized the sample and excites the resulting atoms or ions. The atoms or ions emit particular light which is then transformed to electrical signals. By comparing the intensity of the electric signal of unknown sample to that of sample with known concentration, the material and its concentration can be determined. (Upcommons.upc.edu, 2018) The analysis is performed on aqueous solution sample. Acid digestion is often required for more effective elemental analysis (Norris, 2017).

ICP-OES analysis was carried out to study the bulk composition of the spent catalyst samples. The measurement was carried out using a PerkinElmer optical emission spectrometer Optima 7000 DV with argon gas as plasma. Since the samples introduced into the ICP-OES must be in liquid form, the spent catalyst samples were first digested in 8M of HNO_3 to release the metal elements into solution. The resulting solutions were then diluted with deionised water to obtain concentration of 100 ppm. The standard solution of nickel was prepared at concentration of 5, 15, 25, 50 and 100 ppm. Blank solution used in this analysis was deionised water. The actual concentration of nickel in the spent catalyst samples were determined from this range of standard using the calibration curve obtained. The preparation of standard solution is attached in Appendix A. A wash time of 120 s was required prior to each analysis. For better accuracy, three readings were taken for each sample.



Figure 3.11: PerkinElmer optical emission spectrometer Optima 7000 DV

CHAPTER 4

RESULTS AND DISCUSSION

4.1 Weight Loss of Spent Catalysts Before and Roasting

The catalysts collected from hydrogenation process were first washed with acetone at room temperature to remove residual fats and oils coated on the catalysts surface. The acetone-washed spent catalysts were then subjected to roasting in a furnace with temperature of 350 °C for 3 hours. The weight of the spent catalysts from different organic samples before and after calcinations were recorded and shown in Table 4.1.

The weight loss of the spent catalysts after roasted is possibly caused by the removal of water and volatile compounds. During hydrogenation of organic mediums, hydrocarbons are adsorbed on the catalyst surface and some are retained in the pores and cavities of the catalyst. Besides that, carbonaceous materials may be formed during hydrogenation involving hydrocarbons. Hence, the weight loss can also be caused by the decomposition or oxidation of the coke compounds. Table 4.1 also shows that weight yield of spent catalyst from hydrogenation of CPO is lowest, and this can be attributed to difficulty in retaining the particles during filtration.

Table 4.1: Weight of spent catalyst before and after

Sample	Weight before roasting (g)	Weight after roasting (g)	Weight Loss (g)
Citral	0.1025	0.0788	0.0237
CPO	0.0642	0.0183	0.0459
Lauric Acid	0.1558	0.1381	0.0177
SPSFA	0.1449	0.0725	0.0724

4.2 Characterization of Catalyst

The fresh and roasted acetone-washed spent Ni/SiO₂ catalysts were subjected to characterization in order to investigate the extent of deactivation on the catalysts. The characterization techniques employed were Scanning Electron Microscopy with Energy Dispersive X-ray Spectroscopy (SEM-EDX), and Inductively Coupled Plasma Optical Emission Spectroscopy (ICP-OES). The results obtained from these analyses are presented in the following section.

4.2.1 Scanning Electron Microscopy with Energy Dispersive X-ray Spectroscopy (SEM-EDX)

The surface morphology of the fresh and roasted acetone-washed spent catalysts was observed by employing SEM analysis. Concurrently, the elemental composition on their surface was analysed using EDX. The SEM images of the fresh Ni/SiO₂ catalyst are shown in Figure 4.1. Meanwhile, spent catalysts collected from different hydrogenated organic samples (CPO, lauric acid, SPSFA and citral) are shown in Figure 4.2, Figure 4.3, Figure 4.4 and Figure 4.5, respectively. These SEM images clearly illustrate that the surface of both fresh and spent catalysts is rough and uneven. Besides that, the SEM images show that all the catalysts samples have mostly globular surface which indicates high surface area.



Figure 4.1: SEM image of fresh Ni/SiO₂ catalyst (magnification x5500)

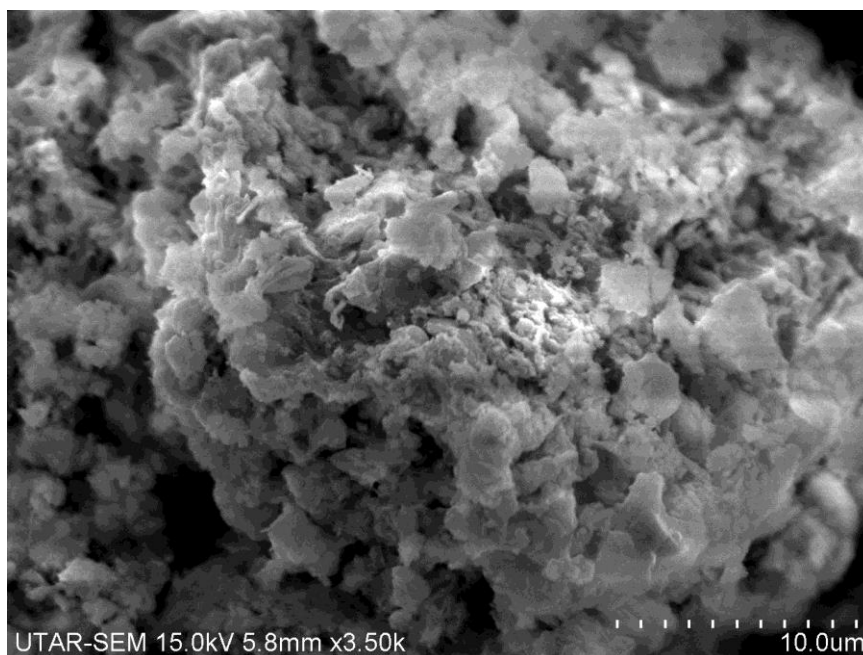


Figure 4.2: SEM image of roasted acetone-washed spent Ni/SiO₂ catalyst collected from CPO (magnification x3500)

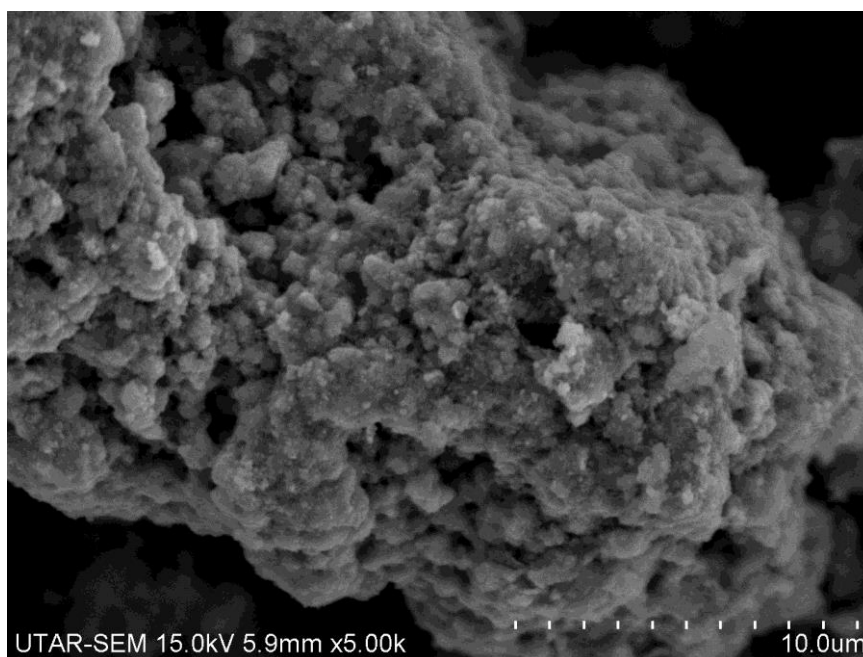


Figure 4.3: SEM image of roasted acetone-washed spent Ni/SiO₂ catalyst collected from lauric acid (magnification x5000)

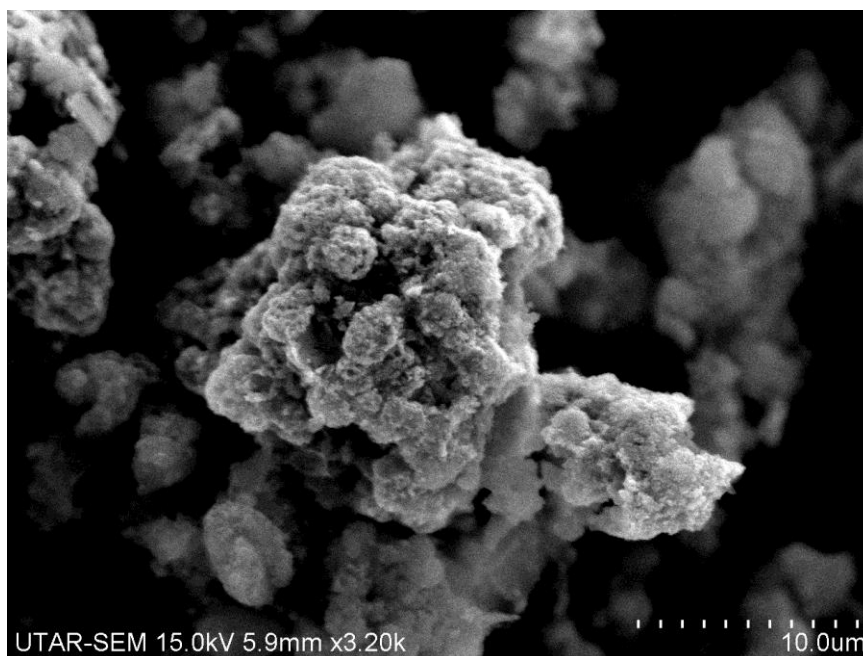


Figure 4.4: SEM image of roasted acetone-washed spent Ni/SiO₂ catalyst collected from SPSFA (magnification x3200)

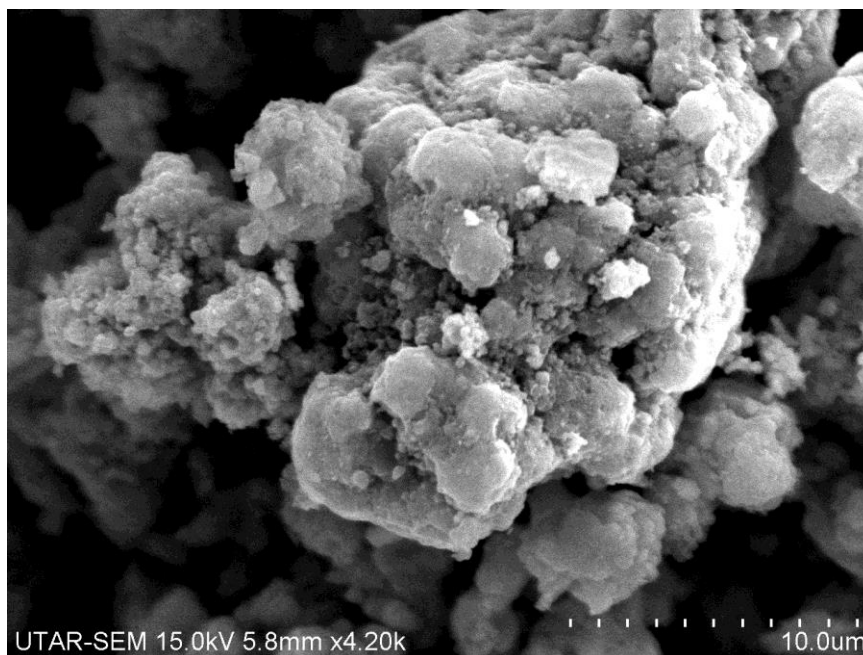


Figure 4.5: SEM image of roasted acetone-washed spent Ni/SiO₂ catalyst collected from citral (magnification x3200)

The average values of the elemental composition of each catalyst sample are shown in Table 4.2 in terms of weight percentage. The results from EDX analysis are taken at three different spots on the same catalyst sample and the raw data is attached in Appendix B. Results in Table 4.2 show high carbon content throughout the spent catalyst samples which indicates that the catalyst surfaces are likely to be covered by coke. This implies that the roasting temperature (350 °C) or roasting time (3 hours) for acetone-washed spent catalysts is insufficient to efficiently remove the residual organic compounds adsorbed on the catalysts, resulting in high carbon loading on the surface of spent catalysts. The catalyst sample from SPSFA in particular shows a significantly higher carbon content. This could be attributed to the higher boiling point of the SPSFA which tends to be trapped in the pores and become difficult to be removed. This again indicates that roasting at 350°C for 3 hours is insufficient to fully remove the carbon materials that could easily accumulate on the spent catalyst sample.

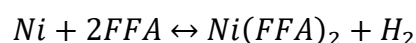
In addition to the carbon content, Table 4.2 also shows that the spent catalyst sample from CPO contains a higher amount of Ca compared to other

samples, which could originate from the higher content of impurity in the CPO. On the other hand, Table 4.2 also shows the amount of nickel dissolved in the hydrogenated organic samples. The nickel loading on the fresh catalyst is 50.99 wt% as shown in Table 4.2. The spent catalyst samples from SPSFA and CPO have the lowest and second lowest amount of nickel which are 44.65 wt% and 32.84 wt%, respectively. This indicates that nickel has dissolved more significantly into CPO and SPSFA as compared to the catalysts in other organic mediums.

Table 4.2: EDX elemental composition of fresh and spent Ni/SiO₂ catalyst collected after the hydrogenation of different organic medium

Element	Fresh	CPO	Lauric acid	SPSFA	Citral
	Wt (%)	Wt (%)	Wt (%)	Wt (%)	Wt (%)
C	13.85	9.60	10.67	23.57	14.71
O	27.34	31.74	28.13	30.55	29.14
Ni	50.99	44.65	49.19	32.84	47.49
Si	7.07	10.76	11.44	12.40	7.92
Ca	0.74	3.25	0.57	0.65	0.74

Ostwald ripening is a sintering deactivation mechanism in which metal atoms tend to dissolve into the surrounding solution and then redeposit onto the surface to form larger particles. However, the significant loss of nickel from 50.99 wt% to 32.84 wt% as seen for catalyst sample in the SPSFA can be attributed to Ostwald ripening instead of particle migration. It is thought that the higher extent of Ostwald ripening in SPSFA is the higher acidity in SPSFA compared to other organic medium which tends to leach the nickel. As the SPSFA is splitted fats, it consists of higher level of free fatty acids than other organic mediums. Being an acid, free fatty acids attacked the nickel nanoparticles during the hydrogenation reaction, resulting in the formation of nickel soaps which are soluble in the fatty acid product and thereby causing deactivation for the catalysts. Free fatty acids react with nickel according to the reaction equation shown below (Padley, 2018):



where Ni is nickel catalyst, FFA represents free fatty acids and Ni(FFA)_2 is nickel soaps where the soap formation follows a saponification process.

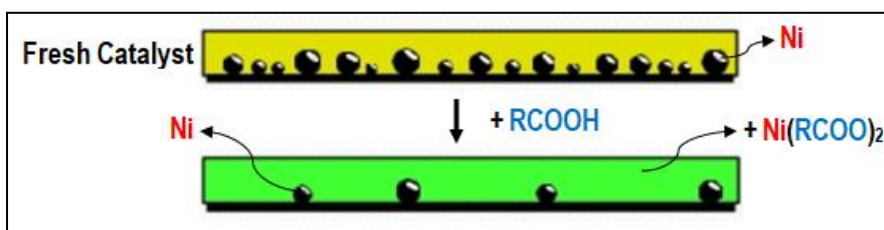


Figure 4.6: Dissolution of Nickel in Fatty Acids (Hawkins, 2013)

However, the nickel loading of the fresh and spent catalysts do not rely solely on the result as presented above as the EDX analysis only focuses on surface instead of the overall bulk catalyst sample. Further clarification of nickel loading for all fresh and spent catalyst samples was conducted by ICP-OES and discussed in the following section.

4.2.2 Inductively Coupled Plasma Optical Emission Spectroscopy (ICP-OES)

The results obtained from ICP-OES analysis are presented in Table 4.3. As the amount for spent catalyst collected from CPO is less than 0.1 g which is the minimum required to obtain 100 ppm sample solution, hence the CPO sample is not subjected to ICP-OES analysis. Based on the ICP-OES results, it is observed that the spent catalyst lost some nickel as compared to that of fresh catalyst. The results are in agreement with the result obtained from EDX analysis where the nickel loading of catalyst samples decreases after subjected to hydrogenation process. Among the different organic mediums, nickel dissolved more significantly in SPSFA and CPO in which the catalyst samples give the lowest and the second lowest amount of nickel loading.

Table 4.3: ICP-OES elemental analysis of spent catalyst sample

Sample	Ni concentration (mg/L)	Percentage Loss of Ni (%)
Fresh	36.35	-
Lauric Acid	28.29	22.17
SPSFA	21.50	40.85
Citral	33.21	8.63

Comparing the results from ICP-OES analysis and EDX analysis, the nickel loadings for EDX analysis are much higher than ICP-OES analysis which may be caused by the nature of analysis. Since EDX technique is employed for surface analysis, it allows higher amount of nickel to be dispersed on the catalyst sample, enhancing the nickel surface enrichment leading to higher nickel loading. Yet, the ICP-OES results represent the overall composition of the catalyst as the measured value is dependent on the dissolved catalyst sample.

4.3 Catalyst Performance Evaluation

Fresh Ni/SiO₂ catalysts were used for hydrogenation of different organic medium as outlined in section 3.2. When the period of reaction was completed, the collected samples were subjected to filtration process to filter off the catalyst within the samples. After that, the liquid samples were left at room temperature. Figure 4.7 to Figure 4.10 show the filtered CPO, lauric acid, SPSFA and citral for hydrogenation conducted with the aid of Ni/SiO₂ catalyst, respectively. At room temperature, the fatty acids samples exhibit a solid form.

By observing the collected CPO samples (Figure 4.7), the colour of unreacted CPO shows orange-red while the colour of hydrogenated CPO samples changed from darker milky green to lighter shade of milky green with the increase of reaction time. For the case of lauric acid, it is white in colour before hydrogenation whereas it showed milky white colour after hydrogenation. The colour of samples changed to lighter shade as reaction time increased. Apart from colour change, the hardness of these samples increased with the increase of reaction time due to

increased percentage of saturated compounds. For example, the sample collected at 3 hour of reaction time is much harder than the other sample collected before 3 hour. On the other hand, there is no visible change in colour and texture for the SPSFA samples.

As for citral, it appears as pale yellow liquid before the hydrogenation while it shows as dark yellow liquid after hydrogenation. However, the colour change for hydrogenated citral samples is not visible after 30 mins.

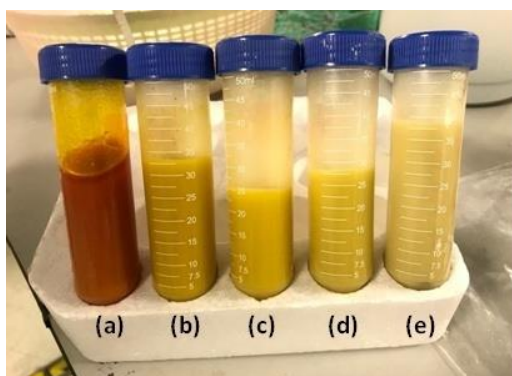


Figure 4.7: Crude Palm Oil (CPO) before (a) and after 30 minutes, 60 minutes, 120 minutes and 180 minutes (b, c, d, e) hydrogenation reaction, respectively.



Figure 4.8: Lauric acid before (a) and after 30 minutes, 60 minutes, 120 minutes and 180 minutes (b, c, d, e) hydrogenation reaction, respectively.

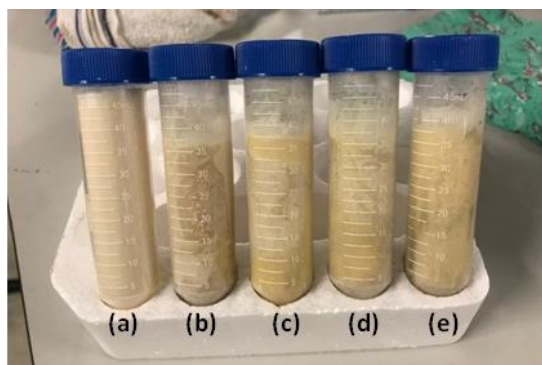


Figure 4.9: Splitted palm stearin fatty acid (SPSFA) before (a) and after 30 minutes, 60 minutes, 120 minutes and 180 minutes (b, c, d, e) hydrogenation reaction, respectively.

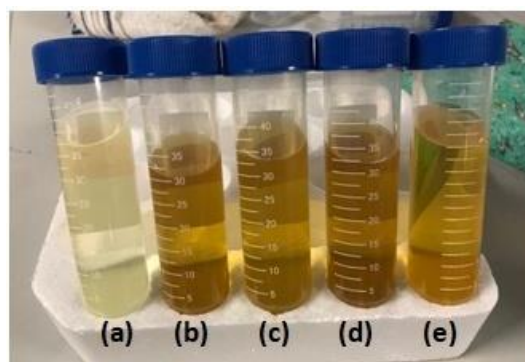


Figure 4.10: Citral before (a) and after 30 minutes, 60 minutes, 120 minutes and 180 minutes (b, c, d, e) hydrogenation reaction, respectively.

4.3.1 Iodine Value (IV)

For fats and fatty acids samples, iodine value test was employed to determine the degree of unsaturation at different time interval. The difference in IV at different reaction time for hydrogenated samples will provide information on catalyst performance. Wijs method was applied to perform the IV test and the collected data were analysed and calculated to the corresponding IV for each sample. Table 4.4 and Figure 4.11 show the results of iodine value test for fatty acids hydrogenated with the aid of Ni/SiO₂ catalysts. Citral was excluded from this test as it does not have any unsaturated double bond. Sample calculation was provided in Appendix C.

Table 4.4: IV test result for CPO, lauric acid, SPSFA hydrogenated in the presence of Ni/SiO₂ catalysts

Time (min)	Iodine Value		
	CPO	Lauric acid	SPSFA
0	41.76	1.39	25.92
30	38.59	0.44	7.70
60	33.37	0.38	5.18
120	28.70	0.25	1.85
180	26.38	0.14	0.37

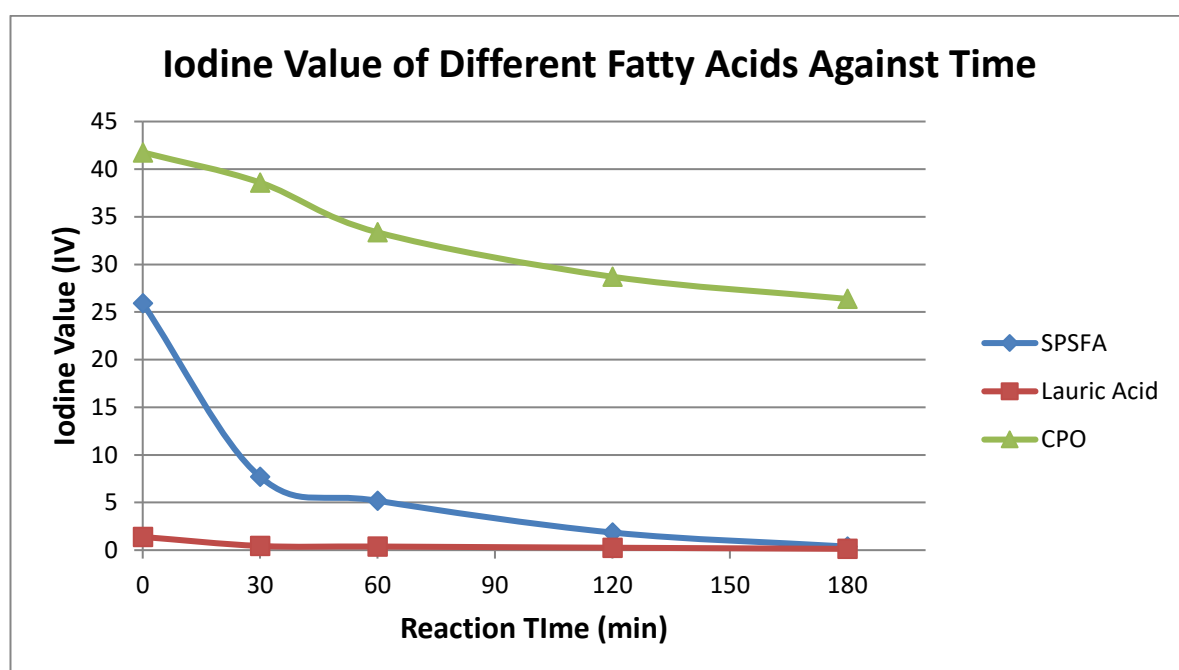


Figure 4.11: IV test result for CPO, lauric acid, SPSFA hydrogenated in the presence of Ni/SiO₂ catalysts

From the results of IV against reaction time, the information about the rate of reaction can be obtained. The gradient of an IV against reaction time graph represents the catalytic activity of a catalyst in which the greater or steeper the gradient, the higher the activity of the catalyst. As observed in Figure 4.11, the catalyst shows the best performance in the hydrogenation of SPSFA. This is because

it exhibits more rapid catalytic activity at the beginning of 30 minutes of the hydrogenation reaction. As can be seen from Figure 4.11, the IV of SPSFA displays a steep drop from 25.92 to 7.70 within the first 30 minutes of reaction. After that, the SPSFA displays a continue drop in IV, and finally was managed to be hydrogenated to the IV of 0.37 at reaction time of 180 minutes. Next to the best is lauric acid. The catalytic activity profile in lauric acid is somewhat similar to that of in SPSFA as it shows significant IV drop which is 1.39 to 0.44 in the first 30 minutes. At the end of the hydrogenation, lauric acid achieved the lowest IV of 0.14 at reaction time of 180 minutes and is comparatively smaller than that achieved by hydrogenated SPSFA.

On the other hand, the IV trend of CPO as shown in Figure 4.11 show a relatively smooth and steady drop which indicates moderate to poor catalytic activity. It has the highest IV of 41.76 in the beginning and decreased to 26.38 at the end of hydrogenation. It appears that the poor catalytic activity for hydrogenation of CPO is most likely due to poisoning and fouling. As evidenced by the EDX data shown in Table 4.2, the fouling could be attributed to the presence of significant amount of calcium (for CPO sample) that slowed down the reaction rate. The high basicity of the calcium compound lead to strong adsorption (Li *et al*, 2017) on catalyst surface resulting in the blockage of active surface area. The reactants were then hindered from accessing to active sites.

Overall, both the SPSFA and lauric acid samples show steep drop in IV especially at the beginning of 30 minutes time interval that represent high activity of the catalyst and their rate of IV drop only slow down after one hour of hydrogenation. The slow down in IV drop indicates that the catalysts could be deactivated. Unlike the case for CPO where there is significant content of calcium that acts as poison for the catalyst, the deactivation of SPSFA and lauric acid will most likely due to Ostwald ripening as discussed in Section 4.2.

In the review by Rekker *et al*. (2013), nickel catalysts are always subjected to rapid deactivation due to extensive crystallite growth by the attacks of free fatty acids. On top of that, the exposure of catalyst to air and water vapour also contribute to the decline in catalytic activity. The oxygen in air and water vapour would act on the active sites, inhibiting the adsorption of reactants (Quincoces *et al.*, 2005).

Therefore, purging out the air and water vapour from the reactor with nitrogen gas is required before the hydrogenation in order to prevent the deactivation caused by air and water vapour. This undesired effect is partially reversible when the oxygen and water vapour are removed by inert calcinations since the active sites are merely covered but not destroyed. One way to hinder the rate of catalyst deactivation is to introduce promoter into nickel catalyst, for example, manganese and copper (Rekker *et al.*, 2013; Bouwman *et al.*, 2011). With the aid to promoter, the nickel catalyst shows higher activity despite a lower specific surface area because of higher turnover number or slower catalyst deactivation (Rekker *et al.*, 2013).

4.3.2 Gas Chromatography (GC) Analysis

Gas chromatography was employed to separate and quantify the components of complex organic chemical mixtures. In the case of CPO, lauric acid and SPSFA, due to the limited volatility of fatty acids, these compounds were esterified to fatty acid methyl esters (FAMES) before subjected to analysis. The fatty acids samples were separated using COL-ELITE-2560 capillary column (100 m × 0.25 mm ID × 0.20 µm df) with a total run time of 58 minutes. The chromatograms obtained present a great amount of peaks which are identified according to the used standards. Table 4.5 abbreviates the percentage composition of fatty acids determined in different organic samples before and after hydrogenation. In the unreacted CPO sample, palmitic acid (C16:0), stearic acid (C18:0), oleic acid (C18:1) and linoleic acid (C18:2) were observed with percentage composition of 43.94 %, 3.48 %, 45.18 % and 7.4 %, respectively. The predominant fatty acids in lauric acid before hydrogenation are 17.08 % of lauric acid (C12:0), 23.43 % of palmitic acid (C16:0) and 6.23 % of stearic acid (C18:0). For SPSFA before hydrogenation, the fatty acids detected are myristic acid (C14:0), palmitic acid (C16:0), stearic acid (C18:0) and oleic acid (C18:1) with percentage composition of 1.65 %, 65.95 %, 30.80 % and 1.59 %, respectively.

Generally, the hydrogenation of fats and fatty acids are a complex network of chemical reactions involving various reactant species and isomers. The several reactant species and isomers compete with each other for the catalyst active sites

(Schneider *et al.*, 2010). Therefore, the hydrogenation reaction forms consecutive saturation of C18:2 to cis-C18:1, and cis-C18:1 to C18:0, as well as the parallel and reversible isomerisation of cis-C18:1 to trans-C18:1 isomers (Schneider *et al.*, 2010). As hydrogenation proceed, the amount of unsaturated fatty acids C18:1 and C18:2 in all three samples decreased while the amount of amount of saturated fatty acids C18:0 increased. The data in Table 4.5 indicates that all the saturated fatty acids except C18:0 remained fairly constant throughout the hydrogenation.

The results obtained from GC analysis relates well with the results from IV test. Referring to Table 4.4 as discussed in Section 4.3.2, the IV of CPO is the highest among the samples which indicates that it exhibits the largest degree of unsaturation. Results from GC analysis also show the highest percentage composition of unsaturated fatty acids in CPO. As for lauric acid, low IV and large amount of saturated fatty acids from GC analysis show that it is highly saturated. Unsaturated fatty acids C18:1 presented in the SPSFA before hydrogenation and was converted into saturated fatty acids C18:0 at the end of hydrogenation. Thus, the IV is relatively high before hydrogenation but drops significantly throughout the hydrogenation reaction.

Table 4.5: Percentage composition of fatty acids present in CPO, lauric acid, SPSFA before and after hydrogenation

Fatty Acids		CPO		Lauric acid		SPSFA	
		Before (%)	After (%)	Before (%)	After (%)	Before (%)	After (%)
Caprylic acid	C8:0	-	-	1.74	1.75	-	-
Capric acid	C10:0	-	-	1.53	1.20	-	-
Lauric acid	C12:0	-	-	17.08	14.21	-	-
Myristic acid	C14:0	-	-	23.43	23.56	1.65	1.42
Pentadecylic acid	C15:0	-	-	0.45	0.58	-	-
Palmitic acid	C16:0	43.94	42.08	43.67	42.21	65.95	63.82
Stearic acid	C18:0	3.48	11.91	6.23	9.80	30.80	34.76
Oleic acid	C18:1	45.18	26.28	-	-	1.59	0.00
Linoleic acid	C18:2	7.40	4.31	-	-	-	-

Table 4.6 shows the percentage composition of citral during hydrogenation at different time interval. The compositions of unreacted citral taken from GC analysis are 50.39 % neral and 48.36 % geranial which are similar to the assays provided by BASF. From Table 4.6, it can be clearly seen that neral and geranial decreased as reaction time increased. Citronellal was formed after 30 minutes of reaction and gradually increased until 60 minutes and then decreased to 11.93 % at the end of hydrogenation. According to the reaction scheme for hydrogenation of citral (Figure 2.18) as shown in Section 2.3.2, hydrogenation of citronellal can lead to citronellol which might be the reason why citronellal decreased after 60 minutes of reaction time. At the end of hydrogenation, 10.29 % of citronellol was formed.

Table 4.6: Percentage composition of citral during hydrogenation at different time interval

Components (%)	Reaction Time (min)				
	0	30	60	120	180
Citronellal	0	12.28	13.92	13.64	11.93
Citronellol	0	0	5.16	7.87	10.29
Neral	50.39	32.16	26.92	24.71	21.79
Geranial	48.36	47.79	47.03	44.71	39.48

CHAPTER 5

CONCLUSION

5.1 Conclusions

In this project, different organic mediums have been hydrogenated with the use of commercial nickel supported on silica catalysts (Ni/SiO₂) to study the extent of Ostwald ripening in these mediums. To supplement the hydrogenation studies, the fresh and spent catalysts have been characterized with several techniques to obtain the information on the state of the catalysts. The products from the hydrogenation were evaluated with IV test and GC to determine the product composition and therefore the catalyst activity and extent of deactivation. The project objectives have been achieved where:

1. Results from IV test and GC analysis of the hydrogenated products have shown that the IV of SPSFA and lauric acid display steep drop at the beginning of reaction and slowed down after 30 mins of reaction. In contrast, the IV drop for CPO was limited but remain steady throughout the reaction. As for the citral, the composition changes from neral to citronellol after hydrogenation. The slowdown in IV drop could be attributed to significant catalyst deactivation.
2. The fresh and spent catalysts were characterized by SEM-EDX and ICP-OES. By comparing the characterization results of fresh and spent catalysts from EDX and ICP-OES analysis, it is found that the loss of nickel is most significant for hydrogenation of SPSFA compared to other organic mediums. This can be attributed to Ostwald ripening as SPSFA consists of higher level of free fatty acids which tends to leach the nickel nanoparticles and form nickel soap. However, the deactivation of catalyst is found to be the most

severe for hydrogenation of CPO, which could be attributed to the presence of high level of calcium that act as the catalyst poison.

5.2 Recommendations for Future Work

This project has covered some important grounds that begin from catalytic hydrogenation of different organic mediums, characterization of catalyst and the catalyst deactivation. Despite this, there is still room for improvement where the recommendations for future work include:

1. Employing additional characterization techniques such as Brunauer-Emmett-Teller (BET) to study specific surface area, pore size and porosity of catalyst, pulse chemisorption to study the metal dispersion and Transmission Electron Microscope (TEM) to study nickel metal particle size.
2. Employ more efficient filtration method to collect spent catalyst from hydrogenated organic samples to make sure the amount of spent catalyst collected is sufficient for further analysis.
3. A higher roasting temperature (> 350 °C) would be necessary to remove the carbon materials in the spent catalyst sample before the characterization.

REFERENCES

- Adibi, P.T.Z. (2014). *Studies of catalyst sintering during operating conditions*. [online] Chalmers University of Technology. Available at: <https://research.chalmers.se/en/publication/197583> [Accessed 20 March 2018].
- Argyle, M. and Bartholomew, C. (2015). Heterogeneous Catalyst Deactivation and Regeneration: A Review. *Catalysts*, 5(1), pp.145-269.
- Aumo, J., Mikkola, J.-P., Bernechea, J., Salmi, T., and Murzin, D. (2005). Hydrogenation of Citral Over Ni on Monolith. *International Journal of Chemical Reactor Engineering*, 3(1).
- Baldan, A. (2002). Review Progress in Ostwald ripening theories and their applications to nickel-base superalloys Part I: Ostwald ripening theories. *Journal of Materials Science*, 37(11), pp.2171-2202.
- Bartholomew, C. (1993). Sintering kinetics of supported metals: new perspectives from a unifying GPLE treatment. *Applied Catalysis A: General*, 107(1), pp.1-57.
- Bartholomew, C. (2001). Mechanisms of catalyst deactivation. *Applied Catalysis A: General*, 212(1-2), pp.17-60.
- Bartholomew, C. and Farrauto, R. (2006). *Fundamentals of Industrial Catalytic Processes*. New Jersey: Wiley.
- Basile, A. and Dalene, F. (2017). *Methanol: Science and Engineering*. Oxford: Elsevier BV.
- Bouwman, H.J. and Terorde, R.J.A.M. (2014). Hydrogenation of fatty acids using a promoted supported nickel catalyst. BASF corporation, US Patent 8,884,042.
- Bergeret, G. and Gallezot, P. (2008). Particle Size and Dispersion Measurements. *Handbook of Heterogeneous Catalysis*.
- Boskovic, G. and Baerns, M. (2004). Catalyst Deactivation. *Chem Inform*, 35(20).
- Campbell, C. (2002). The Effect of Size-Dependent Nanoparticle Energetics on Catalyst Sintering. *Science*, 298(5594), pp.811-814.
- Ezigbo, V.O. and Mbaegbu, E.A. (2016). Extraction of Lauric Acid from Coconut Oil, Its Applications and Health Implications On Some Microorganisms. *African Journal of Education, Science and Technology*, 3(2), pp.
- Flynn, P. and Wanke, S. (1974). A model of supported metal catalyst sintering I. Development of model. *Journal of Catalysis*, 34(3), pp.390-399.
- Forzatti, P. and Lietti, L. (1999). Catalyst deactivation. *Catalysis Today*, 52(2-3), pp.165-181.

Haber, J., Block, J. and Delmon, B. (1995). Manual of methods and procedures for catalyst characterization (Technical Report). *Pure and Applied Chemistry*, 67(8-9), pp.1257-1306.

Hansen, T., DeLaRiva, A., Challa, S. and Datye, A. (2013). Sintering of Catalytic Nanoparticles: Particle Migration or Ostwald Ripening?. *Accounts of Chemical Research*, 46(8), pp.1720-1730.

Hassan, H.A. (2013). Selective Hydrogenation of Citral Over Mesoporous Ru/TiO₂/SiO₂ Catalysts. HASSAN, H. (2018). Graduate School of Engineering and Sciences of İzmir Institute of Technology.

Hawkins, G. (2013). Dissolved Ni Soaps and How To Minimize Them. [online] Slideshare.net. Available at: <https://www.slideshare.net/GerardBHawkins/dissolved-ni-soaps-and-how-to-minimize-them> [Accessed 24 Aug. 2018].

José Luis Contreras and Gustavo A. Fuentes (2012). Sintering of Supported Metal Catalysts, Sintering - Methods and Products, Dr. Volodymyr Shatokha (Ed.), InTech, DOI: 10.5772/33328. Available from: <https://mts.intechopen.com/books/sintering-methods-and-products/sintering-of-supported-metal-catalysts->

Khatab, T., Abdelghany, A. and Soliman, H. (2016). V₂O₅/SiO₂ as a Heterogeneous Catalyst in the Synthesis of bis(indolyl)methanes Under Solvent Free Condition. *Silicon*.

Kistamurthy, D., Saib, A., Moodley, D., Niemantsverdriet, J. and Weststrate, C. (2015). Ostwald ripening on a planar Co/SiO₂ catalyst exposed to model Fischer–Tropsch synthesis conditions. *Journal of Catalysis*, 328, pp.123-129.

Leofanti, G., Tozzola, G., Padovan, M., Petrini, G., Bordiga, S. and Zecchina, A. (1997). Catalyst characterization: characterization techniques. *Catalysis Today*, 34(3-4), pp.307-327.

Li, X., Li, X., Yang, R. T., Mo, J., Li, J., and Hao, J. (2017). The poisoning effects of calcium on V₂O₅-WO₃/TiO₂ catalyst for the SCR reaction: Comparison of different forms of calcium. *Molecular Catalysis*, 434, 16–24. Lowell, S., Shields, J. and Thomas, M. (2011). *Characterization of porous solids and powders*. Dordrecht: Springer.

Moulijn, J.A. (1993). Catalysis - An Integrated Approach to Homogeneous, Heterogeneous and Industrial Catalysis. *Studies in Surface Science and Catalysis*, 79(C), pp.363-400.

Moulijn, J., van Diepen, A. and Kapteijn, F. (2001). Catalyst Deactivation: Is it Predictable? What to Do?. *Applied Catalysis A: General*, 212, pp-3-16.

Myerson, A. (2002). *Handbook of industrial crystallization*. Oxford: Butterworth-Heinemann.

Norris, S. (2017). *How to Prepare Metal Alloy Samples for Analysis by ICP-OES or ICP-MS*. [online] Armi.com. Available at: <https://www.armi.com/blog/how-to-prepare-metal-alloy-samples-for-analysis-by-icp-oes-or-icp-ms> [Accessed 4 Apr. 2018].

Padley, F. (2018). *Lipid Technologies and Applications*. Boca Raton: Routledge.

Quincoces, C., Guerrero, S., Araya, P. and Gonzalez, M. (2005). Effect of water vapor over Pd-Co/SZ catalyst for the NO selective reduction by methane. *Catalysis Communications*, 6(1), pp.75-80.

Rao, C., Muller, A. and Cheetham, A. (2006). *The chemistry of nanomaterials*. Weinheim: Wiley-VCH.

Ratke, L. and Voorhees, P. (2011). *Growth and coarsening*. Berlin: Springer.

Rekker, T. and Terorde, R.J.A.M. (2014). Process for the hydrogenation of fatty acids using a promoted supported nickel catalyst. Basf Corporation, US Patent 8,686,168.

Rouessac, F. and Rouessac, A. (2007) *Chemical Analysis, Modern Instrumentation Methods and Techniques*, 2nd ed. John Wiley: West Sussex, England.

Saib, A., Borgna, A., Vandeloostrecht, J., Vanberge, P. and Niemantsverdriet, J. (2006). XANES study of the susceptibility of nano-sized cobalt crystallites to oxidation during realistic Fischer–Tropsch synthesis. *Applied Catalysis A: General*, 312, pp.12-19.

Schneidera, R.C., Laraa, L.R.S. and Martinelli, M. (2010). An alternative process for hydrogenation of sunflower oil. *Orbital Elec. J. Chem.*, Campo Grande, 2(2), pp.189-200.

Simonsen, S., Chorkendorff, I., Dahl, S., Skoglundh, M., Sehested, J. and Helveg, S. (2011). Ostwald ripening in a Pt/SiO₂ model catalyst studied by in situ TEM. *Journal of Catalysis*, 281(1), pp.147-155.

Tesisenred.net. (2018). *Characterization Techniques*. [online] Available at: <http://www.tesisenred.net/bitstream/handle/10803/8595/13.pdf?sequence=16> [Accessed 3 Apr. 2018].

Trimm, D. (1977). The Formation and Removal of Coke from Nickel Catalyst. *Catalysis Reviews*, 16(1), pp.155-189.

Upcommons.upc.edu. (2018). *Analytical Techniques*. [online] Available at: <https://upcommons.upc.edu/bitstream/handle/2117/93737/08CAPITOL6.pdf?sequence=8&isAllowed=y> [Accessed 3 Apr. 2018].

Berg, V.D.R. (2016). *Formation, Activity and Growth of Copper Nanoparticles in Methanol Synthesis Catalysts*. [online] Utrecht University Repository. Available

at:<https://dspace.library.uu.nl/bitstream/handle/1874/331047/vdBerg.pdf?sequence=1&isAllowed=y> [Accessed 20 March 2018].

Viswanatha, R. and Sarma, D. (2007). Growth of Nanocrystals in Solution. *Nanomaterials Chemistry*, pp.139-170.

Werz, T., Baumann, M., Wolfram, U. and Krill, C. (2014). Particle tracking during Ostwald ripening using time-resolved laboratory X-ray microtomography. *Materials Characterization*, 90. pp.185-195.

Yao, J., Elder, K., Guo, H. and Grant, M. (1993). Theory and simulation of Ostwald ripening. *Physical Review B*, 47(21), pp.14110-14125.

Zaera, F. and Ma, Z. (2006). Characterization of Heterogeneous Catalysts. *Surface and Nanomolecular Catalysis*, pp.1-38.

APPENDICES

APPENDIX A: Preparation of Solutions Used in ICP-OES

1. Preparation of 8M HNO₃

Molarity of 65 % HNO

$$= \frac{\text{Density of HNO}_3}{\text{Molecular Weight of HNO}_3} \times 0.65 \times 1000$$

$$= \frac{1.4090 \text{ g/cm}^3}{63.0130 \text{ g/mol}} \times 0.65 \times 1000$$

$$= 14.53 \text{ mol/L}$$

$$= 14.53 \text{ M}$$

$$M_1V_1 = M_2V_2$$

Where

M_1 = concentration of 65% HNO₃

V_1 = volume of 65% HNO₃

M_2 = concentration of 8M HNO₃

V_2 = volume of 8M HNO₃

$$M_1V_1 = M_2V_2$$

$$(14.53 \text{ M})V_1 = (8 \text{ M})(1000 \text{ mL})$$

$$V_1 = 550 \text{ mL}$$

Thus, 550 mL of 65% HNO₃ was diluted to 1000 mL with deionised water.

2. Preparation of Stock Solution of Nickel, Ni

$$\begin{aligned} \text{Molecular weight of } Ni(NO_3)_2 \cdot 6H_2O \\ &= 58.693 + 2(14) + 12(15.999) + 12(1.0079) \\ &= 290.7758 \text{ g/mol} \end{aligned}$$

$$100 \text{ ppm of stock solution for Ni} = 100 \text{ mg/L} = 0.1 \text{ g/L}$$

Number of mole of Ni

$$\begin{aligned} &= \frac{0.1 \text{ g/L}}{58.693 \text{ g/mol}} \\ &= 0.0017 \text{ mol/L} \end{aligned}$$

$$\begin{aligned} \text{Mass of } Ni(NO_3)_2 \cdot 6H_2O \\ &= 0.0017 \text{ mol/L} \times 290.7758 \text{ g/mol} \\ &= 0.4943 \text{ g/L} \end{aligned}$$

Thus, 0.4943 g of $Ni(NO_3)_2 \cdot 6H_2O$ was transferred into 1000 mL volumetric flask and top up with deionised water.

3. Preparation of Standard Solution of Nickel, Ni

$$M_1V_1 = M_2V_2$$

Where

M_1 = concentration of stock solution (100 ppm)

V_1 = volume of stock solution

M_2 = concentration of standard solution (5, 15, 25, 50 ppm)

V_2 = volume of standard solution

$$(100 \text{ ppm})V_1 = (50 \text{ ppm})(100 \text{ mL})$$

$$V_1 = 50 \text{ mL}$$

Thus, 50 mL of stock solution for Ni was dissolved in 8M HNO_3 then diluted to 100 mL with deionised water to produce 50 ppm standard solution of Ni.

4. Preparation of 100 ppm sample solution

$$\begin{aligned} 0.01 \text{ g sample in } 100 \text{ mL} &= \frac{0.01 \text{ g}}{100 \text{ mL HNO}_3} \\ &= \frac{10 \text{ mg}}{0.1 \text{ L HNO}_3} \\ &= 100 \text{ mg/L} \\ &= 100 \text{ ppm} \end{aligned}$$

Thus, 0.01 g of sample was dissolved in 100 mL of 8M HNO₃ to produce 100 ppm sample solution.

APPENDIX B: Raw Data of EDX

APPENDIX C: Calculation for Amount of Fatty acids Required and IV Test

Formula:

$$Iodine\ Value = \frac{(B - S) \times N \times 12.691}{mass\ of\ sample\ (g)}$$

Where

B = volume of sodium thiosulphate used for blank (mL)

S = volume of sodium thiosulphate used for sample (mL)

N = normality of sodium thiosulphate used (0.1 N)

Sample Calculation for SPSFA before hydrogenation

$B = 26.1$ mL

$S = 14$ mL

$mass\ of\ sample\ tested = 0.5925$ g

$$Iodine\ Value = \frac{(26.1 - 14)mL \times 0.1 \times 12.691}{0.5925\ g}$$

$$= 25.92$$

Table C.1: IV Test Results

	Sample								
	CPO			Lauric Acid			SPSFA		
B (mL)	32.8			25			26.1		
Time (min)	S (mL)	Weight (g)	IV	S (mL)	Weight (g)	IV	S (mL)	Weight (g)	IV
0	16.6	0.4923	41.76	24.1	0.8233	1.39	14	0.5925	25.92
30	13.3	0.6413	38.59	24.7	0.8660	0.44	22.3	0.6263	7.70
60	13.1	0.7493	33.37	24.7	1.0001	0.38	23.2	0.7101	5.18
120	12.9	0.8778	28.77	24.7	1.5031	0.25	25	0.7550	1.85
180	9.2	1.135	26.38	24.8	1.8450	0.14	25.7	1.3556	0.37